

Universitat Politècnica de Catalunya
Facultat de Matemàtiques i Estadística

Master in Advanced Mathematics and Mathematical Engineering
Master's thesis

Data-driven model of endogenous and exogenous electric fields modulation of cerebral cortex activity

Jaume Colom Hernandez

Supervised by Alain Destexhe (CNRS, Paris), Mavi Sanchez-Vives (IDIBAPS, Barcelona)

June, 2021

In the first instance I want to thank to Juanjo Rué for letting me have a taste of real mathematics and accepting me as a student in the MAMME, even though I didn't have a mathematics background. During the masters I discovered the interesting field of computational neuroscience through the Mathematical Models for Biology subject, I want to thank Toni Guillamón for his job at teaching the subject and for being an advisor to this thesis as well.

The discovery of neuroscience ignited a curiosity in me that led to a path of learning and self-studying about the topic, which culminated in me deciding I wanted to do the final master thesis in this area. Next, I want to thank Mavi Sánchez and Alain Destexhe for both accepting me as a student in their laboratories and supervising me during this whole process.

I also want to thank all the friends I met during my time in Paris, they have made this time more amenable and we all know we will be in contact for a long while. And last and most important, I want thank my parents for everything they have done.

Abstract

This work aims to introduce and study a mathematical model of the brain cortex, that shows the oscillation (synchronisation) behaviour of the brain via the influence of internal (endogenous) and external (exogenous) electric fields. The model is based on semi-analytic approach combining analytic solutions and numerical methods to model the Up/Down states of the cerebral cortex. It shows how the ephaptic coupling is capable of inducing synchronisation in the brain and how we can simulate the effects of the endogenous currents with an externally applied current, using DC electrodes. It implements numerical simulations for both the model, data analysis/signal processing and parameter search for the model. The model is capable of reproducing experimental results, with constant and rotated electrical fields. It also shows, on the basis of computer simulations, a new approach for the change of state from synchronised to asynchronous irregular state.

Keywords

neuroscience, computational neuroscience, numerical simulations, cerebral cortex, neuron synchronisation, mean-field models

Contents

1	Introduction	4
2	Theory: computational neuroscience	6
2.1	Background	6
2.2	Hubel and Wiesel Experiment	6
2.3	Neural cells and the anatomy of neurons	6
2.4	Mathematical models of neurons	9
3	Theory: Neuronal populations and mean-fields	11
3.1	Neuronal populations	12
3.1.1	Homogeneous population of integrate-and-fire networks	12
3.2	From Microscopic to Macroscopic	13
3.2.1	Activity of a fully connected network	14
3.2.2	Example: Leaky integrate-and-fire model with diffusive noise	14
3.3	Dynamic neural models and the Fokker-Planck approach	15
3.3.1	The continuity equation	15
3.3.2	Flux equation with stochastic spike arrival	16
3.3.3	Flux equation with stochastic spike arrival	17
3.3.4	Fokker-Planck equation	18
3.3.5	Network of leaky integrate-and-fire neurons	18
3.3.6	Synchrony, oscillations, and irregularity	19
4	Experimental basis of the model	22
4.1	Context	22
4.2	Methods	22
4.3	Relevant results	22
4.4	Discussion	23
5	Modelling cerebral cortex synchronisation and modulation by EFs	25
5.1	Population model	25
5.2	Ephaptic interaction	26
5.3	About the implementation	27
6	Numerical simulations and observations	28
6.1	Single population with exogenous current (simple U_{ext} addition)	28
6.2	Membrane potential (U_{ext}) - frequency plot	28
6.3	Adaptation study	30

6.4	Changing external current U_{ext}	30
6.5	Oscillating U_{ext}	31
6.6	Two (ephaptically) coupled populations	31
6.7	Coupling coefficient study on two populations	34
6.8	Two coupled populations with exogenous current (U_{ext})	35
7	Data analysis and fitting the model	36
7.1	Data analysis	36
7.2	Fitting the model to the data	40
7.2.1	The adaptation equation	40
7.2.2	Noise frequency modulation	40
7.2.3	Parameter search algorithm	40
7.2.3	A problem in the data analysis	44
7.2.4	Putting everything together	44
7.2.5	The results	45
8	Conclusions	48
A	Mean-field model (original) parameters	53
B	Averaged recording results	54
C	Parameter set results	55
D	Mean-field model implementation	56
E	Signal processing methods	58
F	Open access Git repository	60

1. Introduction

The cerebral cortex is formed by circuits of connected neurons in a conductive medium [1]. These are organised into horizontal layers, and radially into cortical columns and mini columns. Cortical areas have specific functions such as movement in the motor cortex, and sight in the visual cortex.

One consequence of the vast recurrent connectivity of the cortex is the ability to initiate and sustain patterned network activity, even in the virtual absence of sensory stimulation, such as during quiescent sleep and anaesthesia [2]. During these quiescent periods, the entire cortex undergoes slow, synchronised transitions between vigorous synaptic activity (Up states) and relative silence (Down states). This cycling (<1 Hz) between Up and Down states constitutes the slow oscillation [3].

Great strides have been made in uncovering the cellular and network mechanisms involved in this widespread phenomenon. Several mechanistic features of the slow oscillation remain to be explored, especially the initiation and termination of Up states and the roles of sub-cortical structures in sustaining and pacing the slow oscillation in the cortex.

The occurrence of the slow oscillation has been well-documented from intracellular and extracellular recording and imaging in various experimental preparations [4], including anaesthetised, naturally sleeping, and quiescent waking animals. The oscillatory rhythm generates extracellular currents and electric fields (EFs) that are prominent enough to be extracellularly measured with local field potentials (LFPs) and also from the skull surface with electroencephalograms (EEGs). Analysis of this type of signals is gaining popularity [5][6] since they carry important information about cognitive and behavioural states [7][8][9][10].

The EFs generated by neuronal activity induce changes in the activity of neurons [11][12], this means that it produces a feedback effect on neuronal activity that shapes and modulates the final network activity [11][12][13][14]. This mechanism is called ephaptic coupling, and it has been known since the 20th century [15]. Cells that are not synaptically connected can interact by means of EFs through the conductive medium [12]. Ephaptic coupling between neurons can end up synchronising networks with a detectable feedback on oscillatory patterns, this is especially evident in the case of epileptic scenarios [16].

Given the impact of slow frequencies on ephaptic interactions [12], there is the hypothesis that slow rhythms may evoke powerful EFs. Exogenous EFs can induce changes in the firing timing of neuronal populations, implying that EF can modulate oscillatory activity [17]. Studies done with exogenous EFs show a critical effect on membrane voltage [11][18][17]. Early studies of the effects of exogenous EFs used strong fields that only occurred under pathological conditions [16]. But, more recent work tackles the case of weaker EFs in the mammalian brain, mostly focused on rodent hippocampus [19][20][21].

What is the interest for studying the slow oscillations in the brain? Well, slow oscillations reassemble the activity pattern during slow-wave sleep [2][22]. And there has been evidence that slow wave sleep plays an important role in memory consolidation [23]. Also there has been work that show memory enhancement after exposure to extra-cranial sinusoidal EFs in the slow oscillation frequency range [24][25].

The development of models is an integral part of neuroscience and related disciplines, such as psychology or cognitive science [26]. Models can provide new and useful insights. They are used to compactly describe large amounts of data. Models provide causal claims about the relation between neural properties and behaviour. They make predictions and thus allow more targeted experiments, and allow for virtual experimentation, making it easier to get intuitions.

There are several approaches to modelling neuronal activity in the brain. A traditional approach is using mechanistic microscopic models where each neuron is treated individually [27], then the results are obtained from the collective data. These models take a bottom-up approach where biophysical descriptions

of the neurons are used to model individual neurons and then they are (sparsely) connected. There are some obvious drawbacks to this methodology, it is computationally expensive to run these simulations with a big number of neurons and (practically) impossible to run with billions of neurons.

Another problem is that many of the brain signals we use are of mesoscopic scale (hundreds of microns to millimetres), in these measurements we are limited to the resolution of the method which represent the averaged activity over a population of neurons [28]. So there is no point in really working with models with finer resolution, as we have no way of checking its correctness and we can't adjust them to the experimental measurements.

The mean-field approach consists of deriving population-level models based on the properties of single neurons and their interactions [28]. Instead of modelling the spike times of a single neuron which belongs to a specific type, let's say pyramidal neuron in frontal cortex, we ask a different question: What is the activity of the neurons in this region? And we can answer this question at an specific spatial resolution, from multiple layers to whole brain scale. There are relevant projects such as the Human Brain Project [29] or The Virtual Brain [30] that take this approach and are successful at reproducing large scale network simulations with the simplified mean-field approach.

This project has been co-directed by Mavi Sanchez, lab leader at the Systems Neuroscience lab at IDIBAPS, and Alain Destexhe, lab leader at Computational Neuroscience lab at CNRS. At Mavi Sanchez' lab, they do experimental research about the electrical activity generated by the cortical network. At Alain Destexhe's lab they work on developing theoretical models and computer simulations to understand from the microscopic (single neurons) to the macroscopic (networks or populations of neurons) aspects of the central nervous system function. The two labs cooperate under the Human Brain Project umbrella, Alain working on the theoretical aspects and Mavi on the experimental part. I have carried out this project during an international exchange in Paris, France.

The project is organised as follows. With the goal in mind of this report being as self-contained as possible, in section 2 and 3 I provide an overview of computational neuroscience, from the basic definition to a description of the mean-fields. Section 4 is a summary of the Rebolledo *et al.* article [31], this article is the initial basis of this project and I find it relevant for the reader to have an understanding of the experiments and the conclusions to continue forward. Section 5 describes the model on which the most of the work of this project has developed. Sections 6 and 7 show the main bulk of the work realised during the internship, which is the study of the model along various parameters, and the fitting of the model to a new set of recordings with the particularity of rotating EFs.

2. Theory: computational neuroscience

The scientific area now commonly called computational neuroscience uses distinct techniques and asks specific questions aimed at advancing our understanding of the nervous system. A brief definition [27] might be:

Computational neuroscience is the theoretical study of the brain used to uncover the principles and mechanisms that guide the development, organisation, information-processing and mental abilities of the nervous system.

2.1 Background

The term 'Computational neuroscience' was coined by Eric L. Schwartz, to provide a review of a field at a conference, which until that point was referred to by a variety of names, such as Neural modelling, Brain theory, or Neural Networks. Later, Hubel & Wiesel studied the working of neurons across the retina, in the primary visual cortex (the first cortical area) [32]. Further, with the rise in computational power, most computational neuroscientists collaborate closely with experimentalists in analyzing different data and synthesizing new models of biological phenomena.

Neuroscience encompasses approaches ranging from molecular and cellular studies to human psychophysics and psychology. The aim of computational neuroscience is to describe how electrical and chemical signals are used in the brain to interpret and process information. This intention is not new, but much has changed in the last decade. More is known now about the brain because of advances in neuroscience, more computing power is available for performing realistic simulations of neural systems, and new insights are being drawn from the study of simplified models of large networks of neurons.

2.2 Hubel and Wiesel Experiment

This experiment [32] has laid the foundation for exploring computational neuroscience in depth. Professors **David Hubel and Torsten Wiesel** in the 1950s recorded the neuronal activities of the cat across the retina, as they moved a bright light. They filed some exciting observations while the experiment was going on:

- Neurons fired only in some instances, but not always.
- The activity of neurons changed depending on the orientation and location of the line of light.

The electrical and chemical signals recorded in the cells connecting the retina to the brain were converted to sound signals. These sound signals were then played, which resulted in crackling sounds. These were not continuous, instead played only when the neuron fired. Henceforth, it has established a fundamental understanding of how neurons extract the information cast by the retina, and then clearly explained how the visual cortical neurons (present in the primary visual cortex, V1, in the brain) can formulate an image.

2.3 Neural cells and the anatomy of neurons

The brain can be broken down into individual discrete parts called neurons. There're many neuronal shapes possible, i.e. in the visual cortex the neuron is pyramidal, or in the cerebellum they are the Purkinje cells.

Structure of neurons

A neuron consists of three main parts namely Soma, Dendrites, and Axon. Soma is the cell body. Dendrites are the input ends of the neurons whereas the axon is the output end. So, the input is received by the dendrites from the axons of the adjacent neuron. These inputs give rise to an Excitatory Post-Synaptic Potential (EPSP), and when taken as a combination from several other neurons, it provides an Action Potential or a Spike. This spiking happens only when the input reaches a certain threshold.

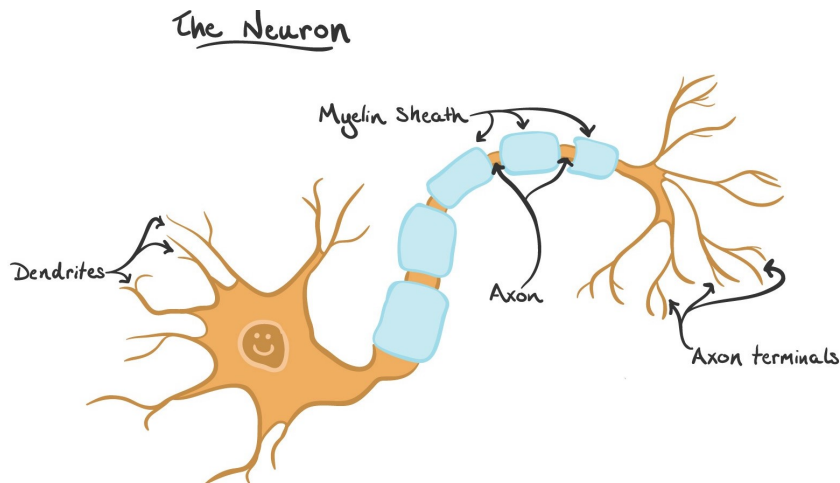


Figure 1: Structure of the neuron. Source: [33]

Going deeper

Neurons deal entirely with chemicals, and chemical reactions drive all the spikes and synapses. We indeed have Na^+ , Cl^- , K^+ and other ions and neurotransmitters in our brains. Contents of a neuron are enclosed within a lipid bilayer, and the lipid is “fat” in simple terms. This bilayer is impermeable to charged ions, such as Na^+ , K^+ , Cl^- , etc. So, how do these chemicals move among the neurons?

The “Ionic Channels” allow the transmission of these ions, i.e., to pass in and out of the neurons. This results in a Potential Difference which exists between the insides and the outer part of the neuron, the inside potential is -70mv relative to the outside.

We have Na^+ , Cl^- on the outside, whereas K^+ , Organic Anion- are present in the inside of a neuron. Vice-versa is possible too, but the ionic concentrations are lower in that case.

Why is the resting potential at -70mv? This is maintained by pumping the ions in and out of the neurons, i.e., by expelling Na^+ out and allowing K^+ in. Ionic channels permit only specific neurons to pass and can be classified into three gated channels.

- **Voltage-Gated** - Probability of opening the channel depends on membrane voltage.
- **Chemically Gated** - Binding to a chemical causes the channel to open.
- **Mechanically gated** - Pressure or stretch influences the channel to open/close

Neuronal signaling (synaptic)

Neuronal signaling is the interaction that happens among the neurons by the transmission of the signals.

The gated channels discussed above allow for neuronal signaling.

- First, the inputs from other neurons activate the chemically gated channels, i.e open the channels, which lead to changes in the local membrane potential.
- Next, this leads to the opening/closing of voltage-gated channels resulting in **Depolarization**(a positive change in voltage) and **Hyperpolarization**(a negative change in voltage). **Repolarization** is where the cell is brought back to the actual potential.
- A strong enough depolarisation will lead to the spike/action potential. This indeed opens the Na^+ channels(voltage-gated), followed by rapid Na^+ influx(out to in) which drives more channels to open until they inactivate.
- When slowly the Na^+ channels start to inactivate, K^+ outflux(in to out) restores membrane potential or the K^+ channels open, reducing the spike. This is Repolarization.
- Thereafter, the cell is made more negative as the K^+ channels stay open and continue to let the positive ions exit the neuron. This is termed as Hyperpolarization.
- As the potassium channels close, the sodium-potassium pump works to reestablish the resting state again.
- After the spike is generated, it is propagated along the axon. Along the axon, Na^+ channels open first, causing the rise of the Action Potential, followed by the closing of the Na^+ channels and the opening of the K^+ channels, which lead to the fall of Action Potential.

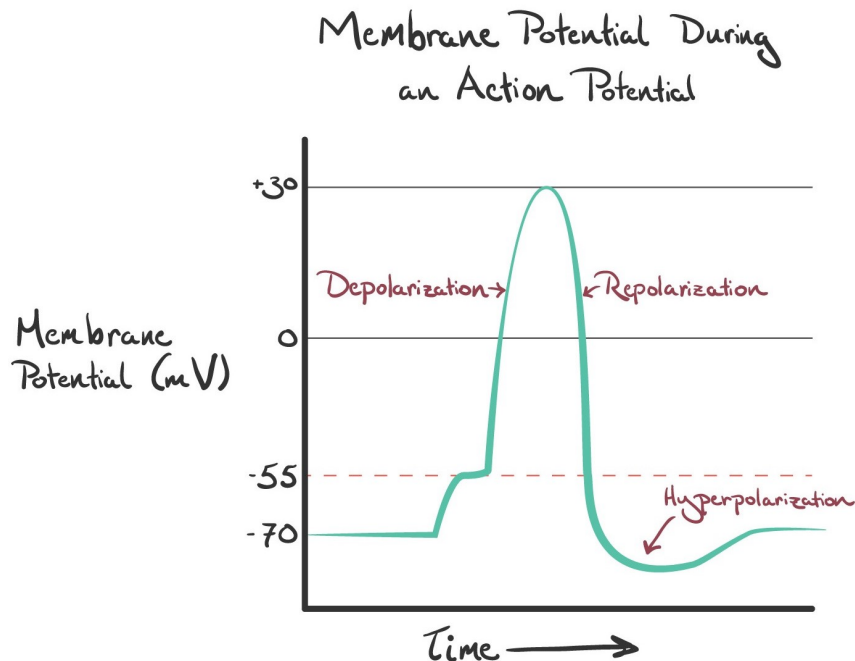


Figure 2: Membrane potential during an action potential. Source: [33]

2.4 Mathematical models of neurons

In this project we do not work on single neuron models, still for sake of completeness I decided to include a small section with description of some mathematical models.

Hodgkin-Huxley Model

The Hodgkin-Huxley model [34] is a model that describes how the potentials are initiated and transmitted in the neurons. It consists of a set of non-linear differential equations describing the behaviour of ion channels that permeate the cell membrane of the squid giant axon. Hodgkin and Huxley were awarded the 1963 Nobel Prize in Physiology or Medicine for this work.

The voltage-current relationship is noted, with multiple-voltage dependent currents charging the cell membrane capacity C_m

$$C_m \frac{dV(t)}{dt} + I_{ion} = I_{ext} \quad (1)$$

The total ionic current I_{ion} is the algebraic sum of the individual contributions from all the participating channel types found in the cell membrane:

$$I_{ion} = \sum_k I_k = \sum_k G_k(V_m - E_k) \quad (2)$$

which extends to the following expression for the Hodgkin-Huxley model of the squid axon, which considers calcium, potassium and leak currents.

$$I_{ion} = G_{Na}(V_m - E_{Na}) + G_K(V_m - E_K) + G_L(V_m - E_L) \quad (3)$$

After some further derivations that involve the expansion of the conductances in terms of its maximal conductances and the activation and inactivation fractions, the end model results in:

$$\begin{cases} C \frac{dV}{dt} = -\bar{g}_K h^4 (V - V_K) - \bar{g}_{Na} m^3 h (V - V_{Na}) - \bar{g}_L (V - V_L) + I \\ \frac{dn}{dt} = \alpha_n(V)(1 - n) - \beta_n(V)n \\ \frac{dm}{dt} = \alpha_m(V)(1 - m) - \beta_m(V)m \\ \frac{dh}{dt} = \alpha_h(V)(1 - h) - \beta_h(V)h \end{cases} \quad (4)$$

This model can have a minimum of 20 parameters which one must estimate or measure for an accurate model. In a model of complex systems of neurons, numerical integration of the equations is computationally expensive and simplifications of the model are needed. It is possible to reduce it to two dimensions [35] thanks to the relations which can be established between the gating variables. But even further simplifications are needed for large scale computations, some theoretical models have been developed that balance accuracy with computation ease.

Perfect Integrate-and-fire

One of the earliest models of a neuron is the perfect integrate and fire model (also called non-leaky integrate-and-fire). A neuron is represented by its membrane voltage V which evolves in time during stimulation

with an input current $I(t)$ according

$$I(t) = C \frac{dV(t)}{dt} \quad (5)$$

which is just the time derivative of the capacitance law, $Q = CV$. When an input current is applied the membrane voltage increases with time until it reaches a constant threshold V_{th} at which point a delta function spike occurs and the voltage is reset to its resting potential, after which the model continues to run.

A shortcoming of this model is that it does not describe adaptation or leakage. If the neuron receives a below threshold short current pulse at some time, it will retain that voltage boost forever - until another input makes it fire. This behaviour is not in line with the observed biological neuron characteristic. Some extension are made to this neuron to make it more reasonable from the biological point of view.

Leaky Integrate-and-fire

The leaky integrate-and-fire model adds a "leak" term in the membrane potential equation, reflecting the diffusion of ions through the membrane. The model equations looks like

$$C_m \frac{dV_m(t)}{dt} = I(t) - \frac{V_m(t)}{R_m} \quad (6)$$

where V_m is the voltage across the cell membrane and R_m is the membrane resistance. The biggest disadvantage is that it does not contain neuronal adaptation so that it can't describe and experimentally measured spike train in response to constant input current. This problem can be solved with generalised integrate-and-fire models that also contain one or several adaptation-variables and are able to predict spike times of cortical neurons under current injection to a high degree of accuracy.

Adaptive Integrate-and-fire

Neuronal adaptation refers to the fact that even in the presence of a constant current injection into the same, the intervals between output spikes increase. An adaptive integrate-and-fire neuron model combines the leaky integration of voltage V with one or several adaptation variables [36]

$$\tau_m \frac{dV_m(t)}{dt} = RI(t) - [V_m(t) - E_m] - R \sum_k w_k \quad (7)$$

$$\tau_k \frac{dw_k(t)}{dt} = -a_k[V_m(t) - E_m] - w_k + b_k \tau_k \sum_f \delta(t - t^f) \quad (8)$$

where τ_m is the membrane time constant, w_k is the adaptation current number, with index k , is the time constant of the adaptation current w_k , E_m is the resting potential and t^f is the firing time of the neuron and the Greek delta denotes the Dirac Delta function. As in the other IF neurons, when the voltage reaches the firing threshold the voltage is reset to a value V_r below the firing threshold.

3. Theory: Neuronal populations and mean-fields

This chapter closely follows chapter 12 and 13 from the book *Neuronal Dynamics* [36]. For an extended introduction see also chapters 14 and 15 from the same reference [36], and for a discussion on the topic see [28].

The brain contains million (billions) of neurons organised in different brain areas, subregions, layers, etc. On the previous section we focused on explaining the behaviour and the mathematical description at the single neuron level. For this section we will shift the attention to the collective properties of groups of neurons.

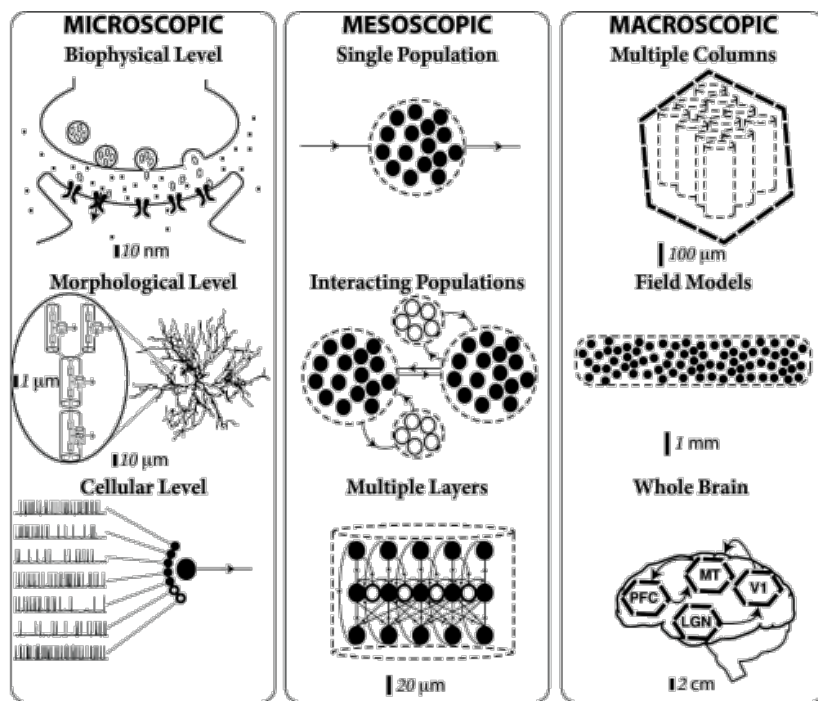


Figure 3: Levels of description and sizes in neuroscience models. Source: [36]

The main idea is shown in Fig 3. Let's show an example, imagine a network of 10000 neurons consisting of 8000 excitatory and 2000 inhibitory neurons that has been simulated while received a time-dependent input. Instead of analysing the spike trains of one or two neurons, we count the number of spikes in a small time step (say $\Delta t = 1\text{ms}$) across all the excitatory neurons in the network. After dividing by the number of (exc.) neurons we get the population activity $A(t)$ of the group of excitatory neurons. In an analogous way we could get the rate of inhibitory neurons.

The central topic of this sections is: Can we predict the population activity $A(t)$ from the properties of its neurons and the network connectivity? How does the population activity respond to novel input?

3.1 Neuronal populations

There are many brain regions where neurons are organised in populations of cells with similar properties. Some examples are columns in the somatosensory and visual cortex and pools of motor neurons. Given the large number and the similarity of the neurons it makes sense to describe the mean activity of the neuronal population rather than the spiking of individual neurons.

First let's define population activity $A(t)$. In a population of N neurons, we calculate the proportion of active neurons by counting the number of spikes $n_{\text{act}}(t; t + \Delta t)$ in a small time interval Δt and dividing by N . Further division by Δt yields the *population activity*

$$A(t) = \lim_{\Delta t \rightarrow 0} \frac{1}{\Delta t} \frac{n_{\text{act}}(t; t + \Delta t)}{N} = \frac{1}{N} \sum_{j=1}^N \sum_f \delta(t - t_j^{(f)}) \quad (9)$$

where δ denotes the Dirac δ function. The double sum runs over all firing times $t_j^{(f)}$ of all neurons in the population. In other words the activity A is defined by a population average. Not to be confused with the mean firing rate of a neuron, defined by temporal averaging in a single neuron. There has been quite some research in the theory of population dynamics, also called neuronal mass models. [37][38][39][40]. The aim is to predict the temporal evolution of the population activity $A(t)$ in large and homogeneous populations of spiking neurons.

3.1.1 Homogeneous population of integrate-and-fire networks

To simplify the study in this section we assume a large and homogeneous population of neurons. By homogeneous we mean that all neurons are identical; all neurons receive the same external input $I_i^{\text{ext}}(t) = I^{\text{ext}}(t)$; the interaction strength w_{ij} for the connectivity between any pair j, i is 'statically uniform', $w_{ij} \approx w_0$, where w_0 is a constant. For $w_0 = 0$ all neurons are independent, and a value $w_0 > 0$ ($w_0 < 0$) implies excitatory (inhibitory) coupling.

In the case of integrate-and-fire neurons, which we have seen in section 1.3, the dynamics are

$$\tau_m \frac{d}{dt} u_i = -u_i + R I_i(t) \quad \text{for } u_i < \vartheta \quad (10)$$

combined with a reset condition: if $u_i > \vartheta$ the integration restarts at u_r . A homogenous network implies that all neurons have the same input resistance R , the same membrane time constant τ_m , as well as identical thresholds ϑ and reset values u_r .

Assuming that a neuron is coupled to all others as well as to itself with coupling strength $w_{ij} = w_0$. The input current I_i is the sum of the external drive and synaptic coupling

$$I_i = \sum_{j=1}^N \sum_f w_{ij} \alpha(t - t_j^{(f)}) + I^{\text{ext}}(t). \quad (11)$$

Here $I^{\text{ext}}(t)$ is the external voltage input at time t and we assume that each input spike generates a postsynaptic current with a generic shape $\alpha(t - t_j^{(f)})$. The sum on the right-hand side of eq. 11 runs over all firing times of all neurons. Because of the homogeneous all-to-all coupling, the total input current is identical for all neurons. Inserting $w_{ij} = w_0$ and using the definition of the population activity, we get the total input current using the activity definition $A(t)$,

$$I(t) = w_0 N \int_0^\infty \alpha(s) A(t - s) ds + I^{\text{ext}}(t), \quad (12)$$

the total input current is independent of the neuronal index i . Therefore, the input current at time t depends on the past population activity and is the same for all neurons.

3.2 From Microscopic to Macroscopic

This will be a first example of how to make the jump from the properties of single spiking neurons to the population activity in a homogeneous group of neurons. It will focus on stationary activity.

If we want to predict the stationary activity in a large network of neurons, then the knowledge of the single-neuron gain function (f - I curve or frequency-current relation) is completely sufficient to predict the population activity.

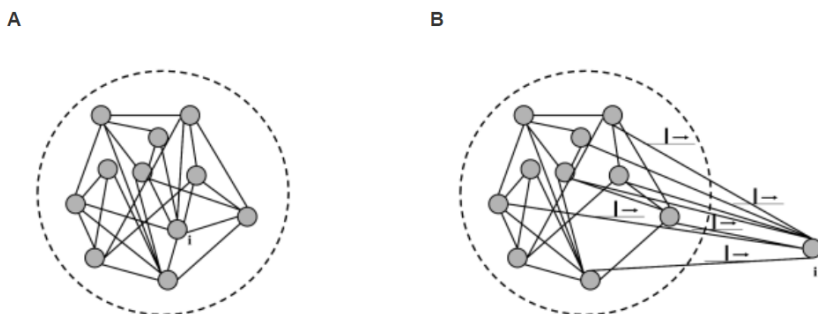


Figure 4: The mean-field argument. **A.** A fully connected population of neurons (not all connections are shown). **B.** Neuron i has been pulled out of the network so as to show that it receives input spikes from the whole population. It is driven by the population activity $A(t)$. The same applies to all other neurons. Source: [36]

In a homogeneous population each neuron receives input from many others, either from the same population or from other populations, or both. Therefore, a single neuron takes as its input a large (and in the case of fully connected network even a complete) sample of the momentary population activity $A(t)$. To keep it simple let's focus on a homogeneous population in a fully connected population, so all neurons are the same and receive the same input.

Under the assumption of stationary network activity, the neurons can be characterised by a constant mean firing rate. In this case, the population activity $A(t)$ must be directly related to the constant single-neuron firing rate ν , so that $A(t) = \nu$. For a proof see chapter 12 section 4 in [36]. This argument is independent of the model neuron choice and holds both for detailed biophysical model i.e. Hodgkin-Huxley or for an AdEx neuron model.

To understand the previous argument let's see an example. Imagine an homogeneous population of $N = 1000$ neurons we observe over a time $T = 10\text{s}$ a total number of 25000 spikes. Under the assumption of stationary activity $A(t) = A_0$ the total number of spikes is $A_0 NT$ so that the population firing rate is $A_0 = 2.5\text{Hz}$. Since all 1000 neurons are identical and receive the same input, the total number of 25000 spikes corresponds to 25 spikes per neuron, so that the firing rate of a single neuron i is $\nu_i = 2.5\text{Hz}$. Thus

$$A_0 = \nu_i \quad (13)$$

The neuron models explained in section 1 enable us to calculate the mean firing rate ν_i for a stationary input, characterised by a mean I_0 and, potentially, fluctuations or noise of amplitude σ . The mean firing

rate is given by the gain function

$$\nu_i = g_\sigma(I_0) \quad (14)$$

where the subscript denotes that the shape of the gain function depends on the level of noise. From the last paragraphs we can conclude that the expected population activity in the stationary state can be predicted from the properties of single neurons.

3.2.1 Activity of a fully connected network

In the previous section we have seen that the firing rate is equivalent to the (expected) value of the population activity A_0 in the state of asynchronous firing. We have then

$$A_0 = g_\sigma(I). \quad (15)$$

The gain function in the absence of any noise ($\sigma = 0$) will be denoted by g_0 .

The total input I to a neuron of a fully connected population consists of the external input $I_{\text{ext}}(t)$ and a component that is due to the interaction of the neurons within the population. The expression of the input current is then

$$I(t) = w_0 N \int_0^\infty \alpha(s) A(t-s) ds + I^{\text{ext}}(t). \quad (16)$$

The overall strength of the interaction is set by w_0 , and $\alpha(s)$ is a postsynaptic current function with normalisation, i.e. $\int_0^\infty \alpha(s) ds = 1$. Now we use the assumption of stationarity and set $\int_0^\infty \alpha(s) A(t-s) ds = A_0$. The left side is the filtered observed quantity, and for a large N we do not have to worry about small fluctuations in A_0 .

Therefore, the assumption of stationary activity A_0 combined with the assumption of constant external input $I_{\text{ext}}(t) = I_0^{\text{ext}}$ yields a constant total driving current

$$I_0 = w_0 N A_0 + I_0^{\text{ext}} \quad (17)$$

Using equation 15 we get an implicit equation for the population activity A_0 ,

$$A_0 = g_0 (J_0 A_0 + I_0^{\text{ext}}). \quad (18)$$

where g_0 is the noise-free gain function of single neurons and $J_0 = w_0 N$. In words, the population activity in a homogeneous network of neurons with all-to-all connectivity can be calculated if we know the single-neuron gain function g_0 and the coupling strength J_0 . This result is independent of any specific assumption about the neuron model.

3.2.2 Example: Leaky integrate-and-fire model with diffusive noise

Let's consider a large and fully connected network of identical leaky integrate-and-fire neurons with homogeneous couplings $w_{ij} = J_0/N$ and normalised postsynaptic currents ($\int_0^\infty \alpha(s) ds = 1$). In the state of asynchronous firing, the total input current driving a typical neuron is then

$$I_0 = I_0^{\text{ext}} + J_0 A_0 \quad (19)$$

In addition, each neuron receives individual diffusive noise of variance σ^2 that could represent spike arrival from other populations. The single-neuron gain function in the presence of diffusive noise is the following

$$A_0 = g_\sigma(I_0) = \left\{ \tau_m \sqrt{\pi} \int_{\frac{u_r - Rl_0}{\sigma}}^{\frac{\vartheta - Rl_0}{\sigma}} \exp(-u^2) [1 + \operatorname{erf}(u)] du \right\}^{-1} \quad (20)$$

with the erf function being $\operatorname{erf}(x) = \frac{2}{\sqrt{2\pi}} \int_0^x \exp(-u^2) du$. In the previous equation σ with units of voltage measures the amplitude of the noise.

3.3 Dynamic neural models and the Fokker-Planck approach

In the previous section we saw the notion of a homogeneous population of neurons. Neurons within the population could be independent, fully or randomly connected, but they should have identical/similar parameters and should receive the same input. Under these conditions it is possible to predict the population activity in the stationary state of asynchronous firing. While the arguments we made in the previous chapter are general they are restricted to the stationary state.

In realistic situations neurons in the brain receive time-dependent input. We change direction of gaze, listen to different auditory stimuli, and touch a variety of different textures with the fingers, not even the body (locomotor system) is in a stationary regime. Indeed electroencephalography recordings from the surface of the human scalp and multi-unit activity recorded from the cortex of animals, indicate that the activity of the brain exhibits a rich temporal structure.

In this section a formulation of population activity that can account for the temporal aspects of population dynamics is presented. It is based on the notion of membrane potential densities for which a continuity equation is derived. Then we study the case for stochastic spike arrival, discuss the Fokker-Planck equation and show the derivation for a network of leaky integrate-and-fire neurons.

3.3.1 The continuity equation

This section shows partial differential equations that describe how the distribution of internal states evolve as a function of time. Since the state of an integrate-and-fire neuron is characterised by its membrane potential, the dynamics of the population are described as the evolution of the membrane potential densities.

Let's start from a homogeneous population of integrate-and-fire neurons. The internal state of a neuron i is determined by its membrane potential which changes according to

$$\tau_m \frac{d}{dt} u_i = f(u_i) + R I_i(t) \quad \text{for } u_i < \theta_{\text{reset}}. \quad (21)$$

Here R is the input resistance, $\tau_m = RC$ the membrane time constant, and $I_i(t)$ the total input (external driving current and synaptic input). If $u_i \geq \theta_{\text{reset}}$ the membrane potential is reset to $u_i = u_r < \theta_{\text{reset}}$. Here $f(u_i)$ is an arbitrary function of u . For $f(u_i) = -(u_i - u_{\text{rest}})$ the equation reduces to the standard leaky integrate-and-fire model.

In a population of N integrate-and-fire neurons, we may ask how many of the neurons have at time t a given membrane potential. For $N \rightarrow \infty$ the fraction of neurons i with membrane potential $u_0 < u_i(t) < u_0 + \Delta u$ is

$$\lim_{N \rightarrow \infty} \left\{ \frac{\text{neurons with } u_0 < u_i(t) \leq u_0 + \Delta u}{N} \right\} = \int_{u_0}^{u_0 + \Delta u} p(u, t) du \quad (22)$$

where $p(u, t)$ is the membrane potential density. The integral over this density remains constant and equal to 1 over time

$$\int_{-\infty}^{\theta_{\text{reset}}} p(u, t) du = 1. \quad (23)$$

Now consider the portion of neurons with a membrane potential between u_0 and u_1

$$\frac{n(u_0; u_1)}{N} = \int_{u_0}^{u_1} p(u', t) du'. \quad (24)$$

The fraction of neurons with $u_0 < u < u_1$ increases if neurons enter across the boundaries. Since N is large it is expected that in a short time interval a big number of neurons cross the boundary u . The flux $J(u, t)$ is the net fraction of trajectories per unit time that crosses the value u . In a finite population of N neurons, the quantity $NJ(u_0, t)\Delta t$ describes the number of trajectories that cross in the interval Δt the boundary u_0 from below, minus the number crossing from above.

Now this is the key step, since trajectories cannot simply end, a change in the number $n(u_0; u_1)$ of trajectories in the interval $u_0 < u_1$ can be traced back to the flux of trajectories in and out of that interval. We therefore have the conservation law

$$\frac{\partial}{\partial t} \int_{u_0}^{u_1} p(u', t) du' = J(u_0, t) - J(u_1, t) \quad (25)$$

Taking the derivative with respect to the upper boundary u_1 and changing the name from u_1 to u yields the continuity equation

$$\frac{\partial}{\partial t} p(u, t) = -\frac{\partial}{\partial u} J(u, t) \quad \text{for } u \neq u_r \text{ and } u \neq \theta_{\text{reset}}, \quad (26)$$

which expresses the conservation of the number of trajectories. In integrate-and-fire models there are two special values where the number is not conserved, u_r and θ_{reset} , because of the fire-and-reset mechanism.

Since neurons that have fired start a new trajectory at u_r , there is a source of new trajectories at $u = u_r$. This can be modelled with a term $A(t)\delta(u - u_r)$ on the right-hand side of the previous expression. The same is added for the Ω_{reset} term. So the expression is

$$\frac{\partial}{\partial t} p(u, t) = -\frac{\partial}{\partial u} J(u, t) + A(t)\delta(u - u_r) - A(t)\delta(u - \theta_{\text{reset}}). \quad (27)$$

The population activity $A(t)$ is the fraction of neurons that fire, i.e. those that pass through the threshold. Therefore we find

$$A(t) = J(\theta_{\text{reset}}, t). \quad (28)$$

The last two equations describe the time evolution of the membrane potential densities and the resulting population activity as a function of time. In the next section we will specify the neuron model to have an explicit expression for the flux.

3.3.2 Flux equation with stochastic spike arrival

Consider the flux $J(u, t)$ in a homogeneous population of integrate-and-fire neurons with voltage equation. We assume that all neurons receive the same current I_{ext} . In addition each neuron receives stochastic background input. An input spike at a synapse of type k causes a jump of the membrane potential by an amount w_k . Example, $k = 1$ could refer to weak excitatory synapses with jump $w_1 > 0$; $k = 2$ strong excitatory synapses with $w_2 > w_1$; and $k = 3$ to inhibitory synapses with $w_3 < 0$. The effective spike arrival rate for each type is ν_k . While the mean spike arrival rates $\nu_k(t)$ are identical for all neurons, we assume that input spike trains at different neurons are independent. Spike arrival can be simulated by independent Poisson processes with rate ν_k .

The flux $J(u, t)$ across a reference potential u_0 can be generated through spike arrivals or through drift caused by the I_{ext}

$$J(u_0, t) = J_{\text{drift}}(u_0, t) + J_{\text{jump}}(u_0, t)$$

and treat each of these in turn.

Since we know that each type of synapse arrives at rate ν_k for each neuron, while the spike trains are independent for different neurons, the total flux caused by input spikes at all synapses can be calculated as

$$J_{\text{jump}}(u_0, t) = \sum_k \nu_k \int_{u_0 - w_k}^{u_0} p(u, t) du. \quad (29)$$

where w_k is the jump cause by a neuron of type k .

The term $J_{\text{drift}}(u_0, t)$ through the reference potential u_0 is given by the density $p(u_0, t)$ at the potential u_0 times the momentary velocity du/dt

$$J_{\text{drift}}(u_0, t) = \frac{du}{dt} \Big|_{u_0} p(u_0, t) = \frac{1}{\tau_m} [f(u_0) + R I^{\text{ext}}(t)] p(u_0, t), \quad (30)$$

where $f(u_0)$ is the non-linearity of the integrate-and-fire model.

3.3.3 Flux equation with stochastic spike arrival

A positive flux through the threshold θ_{reset} yields the population activity $A(t)$. Since the flux has components from drift and from the drift and from jumps, the total flux at the threshold is

$$A(t) = \frac{1}{\tau_m} [f(\theta_{\text{reset}}) + R I^{\text{ext}}(t)] p(\theta_{\text{reset}}, t) + \sum_k \nu_k \int_{\theta_{\text{reset}} - w_k}^{\theta_{\text{reset}}} p(u, t) du. \quad (31)$$

Since the probability density is 0 for $u > \theta_{\text{reset}}$ the inhibitory synapses don't affect the flux.

By inserting the explicit form of the flux into the continuity equation 26 we get the density equation for the membrane potential of integrate-and-fire neurons

$$\begin{aligned} \frac{\partial}{\partial t} p(u, t) &= -\frac{1}{\tau_m} \frac{\partial}{\partial u} \{ [f(u) + R I^{\text{ext}}(t)] p(u, t) \} \\ &\quad + \sum_k \nu_k(t) [p(u - w_k, t) - p(u, t)] \\ &\quad + \tau_m A(t) \delta(u - u_r) - \tau_m A(t) \delta(u - \theta_{\text{reset}}). \end{aligned} \quad (32)$$

The first two terms on the right-hand side describe the continuous drift, the third term the jumps cause by stochastic spike arrival, and the last two terms take care of the reset.

3.3.4 Fokker-Planck equation

The equation for the membrane potential density (32) in a population of integrate-and-fire neurons can be approximated by a diffusion equation, in the limit of small jump amplitudes w_k . To show this, we expand the right-hand side of eq. 32 into a Taylor series up to second order in w_k . The result is the Fokker-Planck equation,

$$\begin{aligned} \tau_m \frac{\partial}{\partial t} p(u, t) = & -\frac{\partial}{\partial u} \left\{ \left[f(u) + R I^{\text{ext}}(t) + \tau_m \sum_k \nu_k(t) w_k \right] p(u, t) \right\} \\ & + \frac{1}{2} \left[\tau_m \sum_k \nu_k(t) w_k^2 \right] \frac{\partial^2}{\partial u^2} p(u, t) \\ & + \tau_m A(t) \delta(u - u_r) - \tau_m A(t) \delta(u - \theta_{\text{reset}}) + \mathcal{O}(w_k^3). \end{aligned} \quad (33)$$

The term with the second derivative describes a 'diffusion' in terms of the membrane potential. Next we define the total drive in voltage units as

$$\mu(t) = R I^{\text{ext}}(t) + \tau_m \sum_k \nu_k(t) w_k \quad (34)$$

and the amount of diffusive noise (in voltage units) as

$$\sigma^2(t) = \tau_m \sum_k \nu_k(t) w_k^2. \quad (35)$$

The firing threshold acts as an absorbing boundary so that the density at threshold vanishes:

$$p(\theta_{\text{reset}}, t) = 0. \quad (36)$$

In order to calculate the flux through the reset threshold we expand in w_k on $u = \theta_{\text{reset}}$ and obtain

$$A(t) = - \frac{\sigma^2(t)}{2\tau_m} \left. \frac{\partial p(u, t)}{\partial u} \right|_{u=\theta_{\text{reset}}}, \quad (37)$$

Eqs 33 - 37 together with the normalisation define the dynamics of a homogeneous population of integrate-and-fire neurons with "diffusive" noise.

3.3.5 Network of leaky integrate-and-fire neurons

In this section we will formulate the interaction between several coupled populations using the Fokker-Planck equation for the membrane potential density and apply it subsequently to the special cases of a population of excitatory integrate-and-fire neurons interacting with a population of inhibitory ones.

Consider multiple populations $k = 1, \dots, K$. The population with index k contains N_k neurons and its activity is denoted by A_k . Recall that $N_k A_k(t) \Delta t$ is the total number of spikes emitted by population k in short interval Δt . Imagine that population A sends spikes to population B . If each neuron in B receive

input from all in A , the total spike rate is therefore $\nu_A = N_A A_A(t)$ ('Full connectivity'). If each neuron in population n receives connections only from a subset of C_{BA} randomly chosen neurons of population k , then the total spike arrival rate is $\nu_A(t) = C_{BA} A_A(t)$. We assume that all connections have the same weight.

For each population $n = 1, \dots, K$ we write down a Fokker-Planck equation analogous to Eq 33. Neurons are leaky integrate-and-fire neurons. Within a population n , all neurons have the same parameters τ_n, R_n, u_r^n and in particular same firing threshold ϑ_n . For population n the Fokker-Planck equation for the evolution of membrane potential densities is then

$$\begin{aligned} \tau_m \frac{\partial}{\partial t} p(u, t) = & -\frac{\partial}{\partial u} \left\{ \left[-u + R_n I_n^{\text{ext}}(t) + \tau_n \sum_k C_{nk} A_k(t) w_{nk} \right] p_n(u, t) \right\} \\ & + \frac{1}{2} \left[\tau_n \sum_k C_{nk} A_k(t) w_{nk}^2 \right] \frac{\partial^2}{\partial u^2} p_n(u, t) \\ & + \tau_n A_n(t) \delta(u - u_r^n) - \tau_n A_n(t) \delta(u - \vartheta_n). \end{aligned} \quad (38)$$

The population activity A_n is the flux through the threshold which in our case

$$A_n(t) = -\frac{1}{2} \left[\sum_k C_{nk} A_k(t) w_{nk}^2 \right] \left(\frac{\partial p_n(u, t)}{\partial u} \right)_{u=\vartheta_n}. \quad (39)$$

The populations interact with each other via the variable $A_k(t)$.

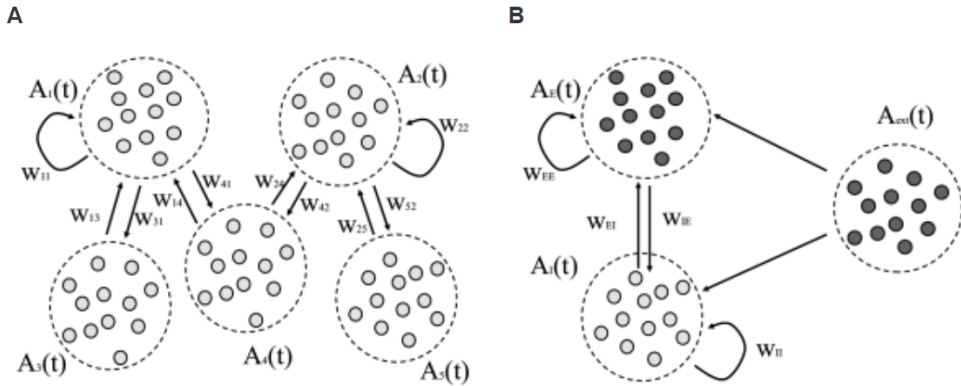


Figure 5: Interacting populations. **A.** Five populations interact with population activities A_k . The parameter w_{nk} gives the synaptic weight of a connection. Not all populations are couples with each other. **B.** Brunel network: An excitatory population of leaky integrate-and-fire neurons is coupled to itself and to an inhibitory population. Neurons in both populations receive also external input from a third population with population activity $A_{\text{ext}} = \nu^{\text{ext}}$ described as a homogeneous Poisson process. Source: [36].

3.3.6 Synchrony, oscillations, and irregularity

With the previous results we can give a complete characterization of a network of leaky integrate-and-fire neurons consisting of two populations, a population of N_E excitatory neurons coupled to a population

with $N_I = N_E/4$ inhibitory neurons. The structure is visualized in Figure 6. Each neuron (excitatory or inhibitory) receives C_E connections from the excitatory population each one with weight $w_{EE} = W_{IE} = w_0$; it also receives $C_I = C_E/4$ connections from the inhibitory and furthermore C_E connections from an external population with neurons that fire at rate ν^{ext} . Each spike causes, after a delay of $\Delta = 1.5\text{ms}$ a voltage jump of $w_0 = 0.1\text{ mV}$ and the threshold is 20 mV above resting potential.

Realise that each neuron receives four times as many excitatory than inhibitory inputs so that the total amount of inhibition balances excitation if inhibition is four times stronger ($g = 4$), but the relative strength g is kept as a free parameter. The weight here has units of voltage and directly gives the amplitude of the voltage jump: $w_0 = \Delta u_E$.

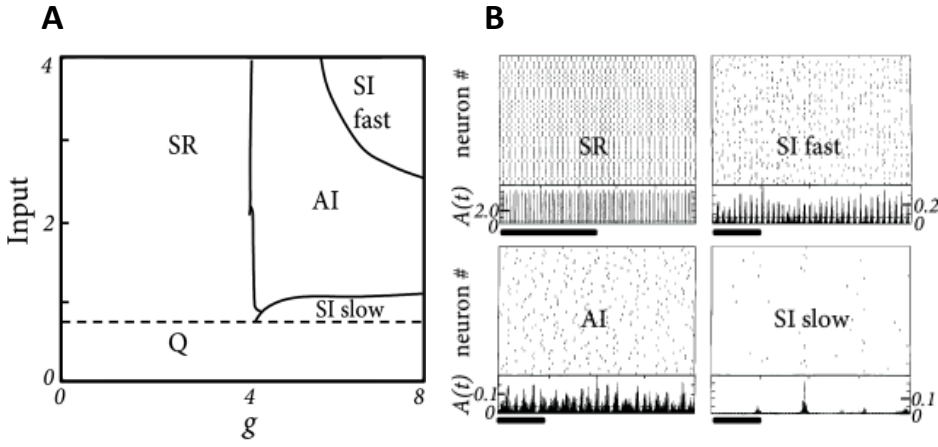


Figure 6: Population of pulse-coupled leaky integrate-and-fire neurons (Brunel network). **A.** Phase diagram of the Brunel network. There are three states, asynchronous irregular (AI), synchronous regular (SR) or synchronous irregular (SI) activity. The horizontal axis indicates the relative importance of inhibition ($g = 4$ corresponds to balance between excitation and inhibition). The vertical axis is the amount of external input each neuron receives. **B.** Typical time course of the population activity $A(t)$ (bottom part of each subgraph, units in kHz) and associated spike patterns. The top part shows the activity of 50 randomly chosen neurons and the bottom part shows the $A(t)$. Source: [36]

The population can be in state of asynchronous irregular activity (AI), where neurons in the population fire at different times ('Asynchronous firing') and the distribution of interspike intervals is fairly broad (irregular firing of individual neurons). With a small change of parameters the same networks can be in a state of fast synchronous regular (SR) oscillations. It is characterised by periodic oscillations of the population activity and a sharply peaked interval distribution of individual neurons. The network can also be in the state of synchronous irregular firing (SI) either with fast (SI fast) or with slow (SI slow) oscillations of the population activity. The oscillatory temporal structure emerges despite the fact that the input has a constant spike arrival rate. It can be traced back to instability of the asynchronous firing regime toward oscillatory activity.

With the Fokker-Planck approach is possible to determine the instabilities analytically. Stability of a stationary state of asynchronous firing is most easily achieved in the regime where inhibition dominates excitation. Since each neuron receives four times as many excitatory as inhibitory inputs, inhibition must be at least four times as strong ($g > 4$) as excitation. In order to get non-zero activity despite the strong inhibition, the external input must be strong enough to make neurons fire.

To understand how the network can run into instability, consider the regime of strong inhibition ($g > 4$)

and strong input. Then a momentary fluctuation may lead to an increase in the total amount of activity in the excitatory population. Then, after a transmission delay Δ an increase in inhibition and, after a further delay Δ a suppression of excitation. If the feedback loop is strong an oscillation with period 4Δ may appear, leading to fast-frequency ('SI fast') oscillations. A similar argument can be made for the 'SI slow' when the external input is weak.

4. Experimental basis of the model

The quantitative model of the Rebolledo *et al.* article [31] is the initial basis for the project, and while we won't perform any experimental (lab) work, it is meaningful to understand the goals, the methodology and the results of this article.

4.1 Context

As explained in the introduction, during deep sleep the cerebral cortex generates periods of activity interspersed with silent periods, these periods are called Up and Down states. This pattern of behaviour is known as slow oscillations (SO).

There are several hypothesis for the origin of these slow oscillations. This publication tackles the problem of understanding how the ephaptic coupling affects the synchronisation, and the modulation properties of the endogenous (self-generated electric fields) currents.

The fact that there is a feedback loop between neuronal activity generated EFs and the impact of those EFs on the neuronal activity, creates an added difficulty to understand the isolated behaviours of the elements. In order to study this behaviour, the researchers have developed the experiments in prepared cerebral cortex slices [4] that allows to manipulate a number of parameters that can't be isolated *in vivo*.

4.2 Methods

To study this behaviour they used 69 ferret cortical slices in different series of experiments. The brain tissue was prepared and inserted in a special bathing medium [31]. The brain tissue was cut in two different parts using a scalpel blade to separate the synaptic from the EF (non-synaptic) activity, the two slices were allowed to be tightly in contact after the cut. In some experiments they introduced a PTFE (teflon) piece in the middle of the two slices.

The recordings were performed with 16 gold electrodes plated with platinum black disposed on a recording grid. The grid and the array of holes was designed and fabricated using SU-8 negative photoresist, as described by [41]. The recording array was placed on top of the slices, obtaining 16 simultaneous recordings, 10 electrodes recorded the left side and 6 the right side.

4.3 Relevant results

Endogenous fields in synaptically disconnected networks

In the first experiment they took measurements from a single piece of brain tissue. There were spontaneously generated slow oscillations with an average frequency of 0.25 ± 0.02 Hz. The oscillations propagated via synaptic connectivity. To cancel the synaptic connectivity they cut the brain tissue in two parts, resulting in two different networks synaptically disconnected. The recordings show how the sectioned slices act like two different oscillators.

To gain better control over the responses of the tissues they triggered network responses with a glutamate injection (local application of 10 to 20 pl of 0.5 mM glutamate) at a frequency similar to the spontaneous slow oscillations (0.25 Hz). The response on the L-side had an amplitude that corresponded to the $4.3 \pm 0.01\%$ of the original response at the R-side. The **peak amplitude decreased with the distance from the original site**: amplitudes were $6.70 \pm 1.06 \mu V$ and $3.54 \pm 0.82 \mu V$ at the L_t -side and

L_d -side, 1.5 and 3 mm apart from the origin site. While the amplitude of the original evoked glutamate response was $529.80 \pm 289.16 \mu V$ at the R-side.

Endogenous fields do not result from chemical propagation nor neuronal firing

To be sure that there was no glutamate diffusion across the cut, the researchers added a piece of Teflon across the two cut sections. This way ruling out the possibility of diffusion. The results were a response of $9 \pm 0.01\%$ which is not significantly different than the one observed in the previous experiment, suggesting that there is no glutamate diffusion across the cut of both sides.

To check if the cut had any effect on the EF propagation, the synaptic activity was blocked with tetrodotoxin (TTX), this drug cancels all the synaptic communication. The responses show that there is no significant difference when applying TTX to the cut network, **so EFs can be generated without requiring amplification by local synaptic activity**.

Endogenous fields affect synaptic activity and rhythmicity

To check whether the endogenous fields modulated the spontaneous slow oscillations, the researchers evoked Up states with glutamate on the right side and took frequency measurements on both sides and using different Up state frequencies (0.66 and 0.33 Hz). The increase (or decrease) of the frequency **induced a parallel increase (or decrease)** in the modulated slow oscillation frequency on the other side. The spontaneous activity was 0.28 Hz on the left side and 0.43 Hz on the right side, and when using the evoked responses on the left side at 0.66 Hz and 0.33 Hz on the right side the responses were 0.77 Hz and 0.23 Hz. The result show that the frequency variation on the R-side is consequence of the frequency variation on the Lt-side and there is a trend towards converging oscillatory frequency.

Relevance of cortical dipoles to EF entrainment of oscillations

Last, the researchers studied how the orientation affected the modulation of the activity. By rotating 180 degrees the R-side, this way the two networks are in contact but with opposite laminar orientation. Under this conditions the EFs were not able to modulate the slow oscillations at the adjacent inverted network. These results show that two adjacent synaptically disconnected networks can only be synchronised by EF when their laminar pattern is similarly oriented.

Next, they took measurements of the fall-off of the evoked potential as a function of the distance. The estimation of the decay with distance matched the $1/r^2$ predicted by electric dipoles. **The decay of the EF response with distance is consistent with the power-law profile predicted by electric dipoles.**

4.4 Discussion

The essence of this article is that endogenous currents create EF strong enough to modulate the contiguous (non-synaptical) neuronal columns. EF modulation of the brain activity in slow oscillations had already been shown by the lab in the publication [42], and also by the literature [2], in the past.

The fact that the results of this publication all derive from the analysis of the ephaptic coupling in the brain tissue, has to be taken into account for the new modelling component of the project. To extrapolate the model to an external EF the component related to the coupling between the different populations will have to be foregone for the new external field, also getting correctly the relationship between the external EF and the impact on the membrane potential ($U_{external}$) will prove one of the hard parts of the project.

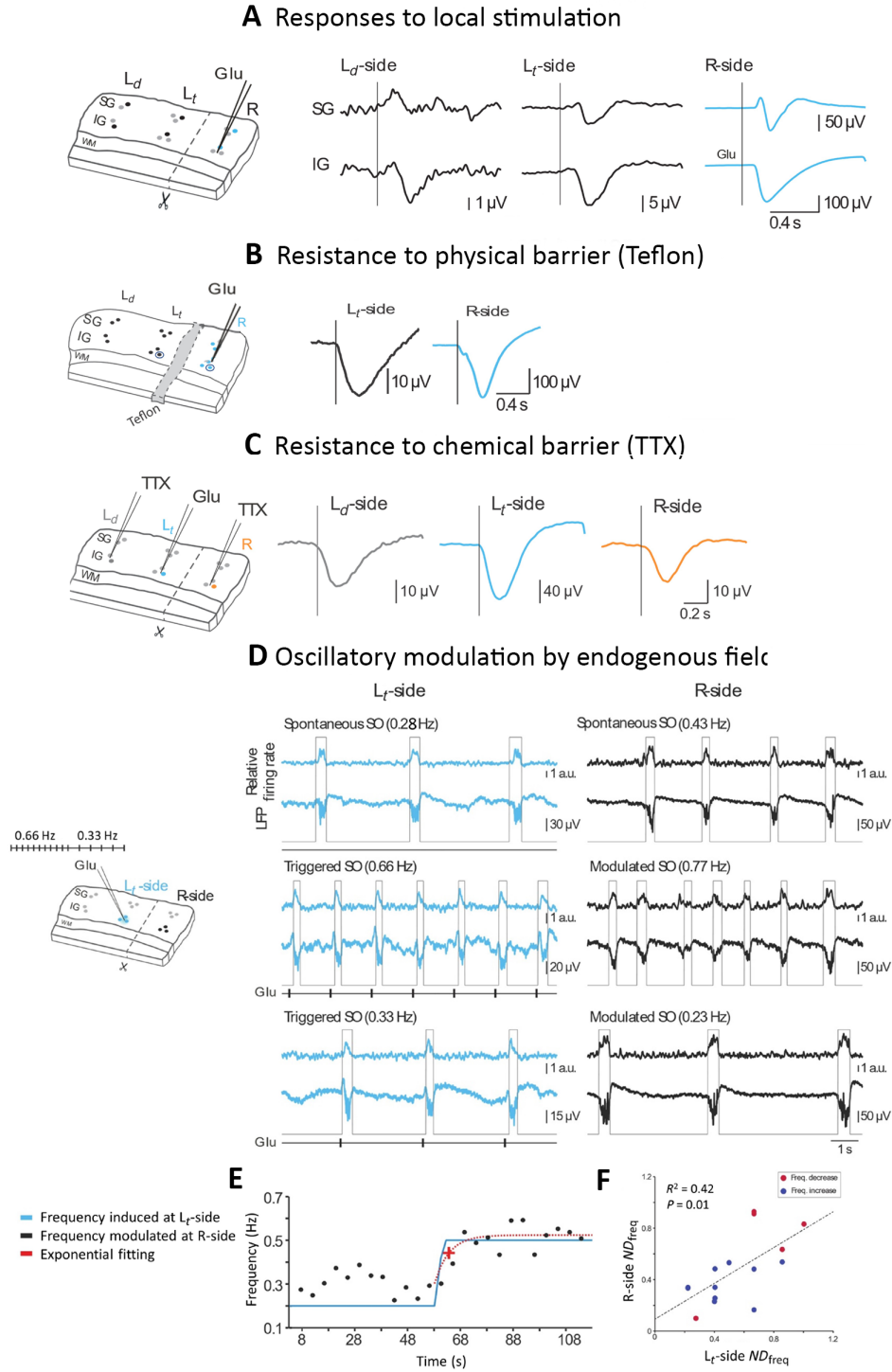


Figure 7: Figures from the Rebollo *et al.* article [31]. (A) Left: Sectioned slice scheme. Right: Glutamate-induced responses on R-side and recorded activity on the L-side. (B) Recordings in the presence of a thin teflon barrier between the two sections. (C) Resistance to an application of TTX to both sides. (D) Relative firing rate and LFP recordings with up/down detector, for the spontaneous SO and the triggered SO at 0.66Hz and 0.33Hz (E) Exponential fitting for a particular frequency change, displaying the frequency modulation. (F) Dispersion plot of the normalised frequencies.

5. Modelling cerebral cortex synchronisation and modulation by EFs

In this section a mean-field model for the activity of the neural populations is presented. The model is based on an hybrid approach. The estimation of the ephaptic coupling coefficient ($\gamma_{ephaptic}$) is done with an analytical solution, and the dynamical solution of the model is based on a numerical solution.

5.1 Population model

The model is an adaptation of a mean-field population model of the network activity [43]. In the first order of approximation, the population dynamics can be described by the mean firing rates of excitatory and inhibitory populations.

$$\tau_e \frac{v_e}{dt} = -v_e + n_e f_e(v_e + v_{ext}, v_i) + \sigma_e \eta_t \quad (40)$$

$$\tau_i \frac{v_i}{dt} = -v_i + n_i f_i(v_e + v_{ext}, v_i) + \sigma_i \eta_t \quad (41)$$

where f_e and f_i are the transfer functions for inhibitory and excitatory neurons, i.e. a function which maps the output firing rate of the neuron to the mean rate of excitatory and inhibitory inputs [28]. n_e and n_i are the sized of excitatory and inhibitory population ($n_e/n_i=4$). In addition to the recurrent inputs from the inhibitory n_i and excitatory n_e populations, excitatory neurons also receive external excitatory inputs v_{ext} . η_t denotes a sample of a non-correlated standard Gaussian noise (white noise), σ_i and σ_e are the SD of the noise for excitation and inhibition. The equations are solved numerically using stochastic Euler method, such that the SD of the (discrete) Gaussian noise was scaled with the square root of the integration time step Δ_t .

The model uses the transfer function proposed by Kuhn *et al.* [44]. It approximated the firing rate of a neuron by a nonlinear function of the membrane fluctuation statistics: mean membrane potential μ_U , SD of membrane potential σ_U and effective membrane time constant τ_{eff} . In the conductance based model they are equal to

$$\langle g_{tot} \rangle = g_I + \langle g_e \rangle + \langle g_i \rangle = g_I + \sum_{s \in \{e, i\}} v_s B_s T_s \quad (42)$$

$$\mu_U = \frac{E_I g_I + E_e \langle g_e \rangle + E_i \langle g_i \rangle}{\langle g_{tot} \rangle} \quad (43)$$

$$\tau_{eff} = C / \langle g_{tot} \rangle \quad (44)$$

$$\sigma_U = \sum_{s \in \{e, i\}} v_s (\tau_{eff} + T_s) \left[\frac{(E_s - \mu_U) B_s T_s \tau_{eff}}{2C(\tau_{eff} + T_s)} \right]^2 \quad (45)$$

Given the analytical statistics, the firing rate can be described by the following non-linear relation

$$f(v_e, v_i; \Omega) = \frac{1}{\tau_{eff}(v_e, v_i)} \text{erfc} \left[\frac{\Theta - \mu_U(v_e, v_i)}{\sqrt{2\sigma_U(v_e, v_i)}} \right] \quad (46)$$

For the inhibitory neurons the threshold for spiking is lower, such that their firing rate is higher than that of the excitatory population. That is the difference between both transfer functions, $f_e(v_e, v_i) = f(v_e, v_i; \theta_e)$ and $f_i(v_e, v_i) = f(v_e, v_i; \theta_i)$.

It was observed [31] that under physiological values of the parameters, the model manifests two stable states: the Up state and the Down state. To obtain the oscillations between these two states adaptation is introduced in the excitatory population, governed by the following dynamic equation

$$\tau_{adapt} \frac{dU_{adapt}}{dt} = -U_{adapt} + \beta_\tau v_{exc} \quad (47)$$

The adaptation parameter β_τ and the SD of noise σ_{exc} were adjusted to match the frequency of the Up state observed in the experiments. The adaptation potential U_{adapt} is subtracted from the mean membrane potential μ_U of the excitatory population, eq. 43.

Up to this moment we have just described a single mean field model. To introduce the relation between different mean field models we add an ephaptic coupling coefficient $\gamma_{ephaptic}$ (V/Hz), which affects the mean membrane potential the following way

$$\bar{\mu}_U^L = \mu_U + \gamma_{ephaptic} v_{exc}^R \quad (48)$$

With this simple mechanism we can model the impact of the coupled mean-field models based on just on their activation rate. All the estimated parameters of the model can be found in A.

5.2 Ephaptic interaction

To estimate the effect of the EF on the membrane depolarization (voltage increase), the theory of linear cable in a polarized extracellular medium. The solution to the cable equation in polarized medium presented by Anastassiou *et al.* [45] is:

$$V_m(X) = -\frac{\Omega^2}{\Omega^2 + 1} \sin(\Omega X + \phi_s) + \frac{\Omega^2}{\Omega^2 + 1} \left(\frac{\cosh(X)}{\tanh(L)} \cos(\phi_s) - \frac{\cosh(X)}{\sinh(L)} \cosh(\Omega L + \phi_s) - \sinh(X) \cos(\phi_s) \right) \quad (49)$$

The solution is given in terms of the dimensionless quantities, defined as

$$\Omega = 2\pi f_S \lambda_{el} X = \frac{X}{\lambda_e l} V_i = \frac{v_i - v_{rest}}{v_0} \quad (50)$$

Then, the extracellular potential is given in terms of harmonic functions

$$v_e = v_0 \sin(\Omega X + \phi_s) \quad (51)$$

Finally, the EF is

$$E - \frac{dv_e}{dx} = -E_0 \cos(\Omega X + \phi_s) \quad (52)$$

To quantify the non-synaptic interaction between two sides of a sectioned slice, the researchers first estimated the magnitude of the EF vector (gradient of electric potential). They stimulated the tissue with a glucamate injection. Assuming that the EF originated from the glucamate injection and was propagated across the cut to the opposite side, we can estimate the magnitude of the related EF vector by taking measures across the radial axis at each lateral position.

The γ_{ephaptic} is estimated from the mean membrane depolarization caused by the ephaptic interaction divided by the mean excitatory population rate in an Up state of an uncoupled model. Using these recorded values in the previous equation the γ_{ephaptic} value of $1/60 \mu\text{V}/\text{Hz}$ is estimated. See A.

5.3 About the implementation

The final model implementation consists of set of three ODEs and the transfer function with the analytical computation of the membrane statistics. The differential equations are integrated using the Euler-Maruyama integration scheme such that the SD of the (discrete) Gaussian noise is scaled with the square root of the integration time step $\Delta_t = 1\text{ms}$.

Algorithm 1: Single population implementation (Stochastic integration)

Result: Time, excitation rate, inhibition rate and adaptation arrays
 model_params \leftarrow Dictionary with all the parameters;
 t, dt, tmax \leftarrow 0, 1ms, 200s;
while $t < t_{\text{max}}$ **do**
 | membrane_statistics \leftarrow compute statistics with parameters (exc_rate, inh_rate,
 | membrane_shift);
 | inhibitory and excitatory freqs \leftarrow transfer function (uses the membrane_statistics);
 | exc_rate, inh_rate, adaptation \leftarrow dynamical equations computation + noise computation;
 | t \leftarrow t+dt
end
 freq, up_period, down_period \leftarrow compute features; /* Optional */

The core implementation of the model can be found at appendix D. And an open access GitHub repository, with ready to run notebooks, is available at F.

6. Numerical simulations and observations

In this section we will show the different experiments we have worked on during the internship and discuss what they mean for the project we have been working on.

6.1 Single population with exogenous current (simple U_{ext} addition)

The first experiment was to run a single mean field and study the behaviour under different constant electric fields. The constant electric field induces a membrane potential shift that is added to the threshold in the transfer function, the same way as with the endogenous EF-currents. So a positive EF pushes the threshold higher augmenting the activity of the mean-field and consequently reducing the periods between peaks.

$$\mu_U = \frac{E_I g_I + E_e \langle g_e \rangle + E_i \langle g_i \rangle}{\langle g_{\text{tot}} \rangle} + U_{\text{external}} \quad (53)$$

In figure 19, we can see 5 different simulations with different U_{external} (external EF). The results are coherent with the expected performance of the model. For positive U_{ext} we see how the mean field has less peaks and is eventually **depressed**, this means that there is no activity on the model. For negative U_{ext} the model has more activity and thus more peaks, and with a very large U_{ext} value the model stays in **asynchronous irregular state (AI)**.

6.2 Membrane potential (U_{ext}) - frequency plot

To measure the impact of having an external EF we compute the frequency of the On/Off states during synchronised activity in the model. There is an almost (inverse) **linear response from $-115 \mu V$ to $80 \mu V$** for the U_{ext} -frequency relationship. For U_{ext} values smaller than $-115 \mu V$ the model starts its transition to AI state, with occasional Off periods and after $-225 \mu V$ the model is completely in AI state. For values higher than $80 \mu V$ the model is in a constant depression state where there is almost no activity.

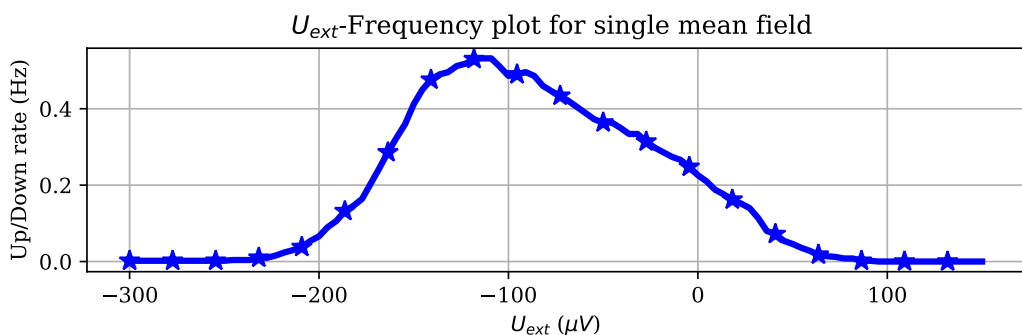


Figure 8: Frequency response to different constant EFs with default parameter mean field. For values between $-200 \mu V$ and $100 \mu V$ the model is in slow oscillations (SO). For smaller values it is asynchronous irregular (AI) and for larger values is in depressed state.

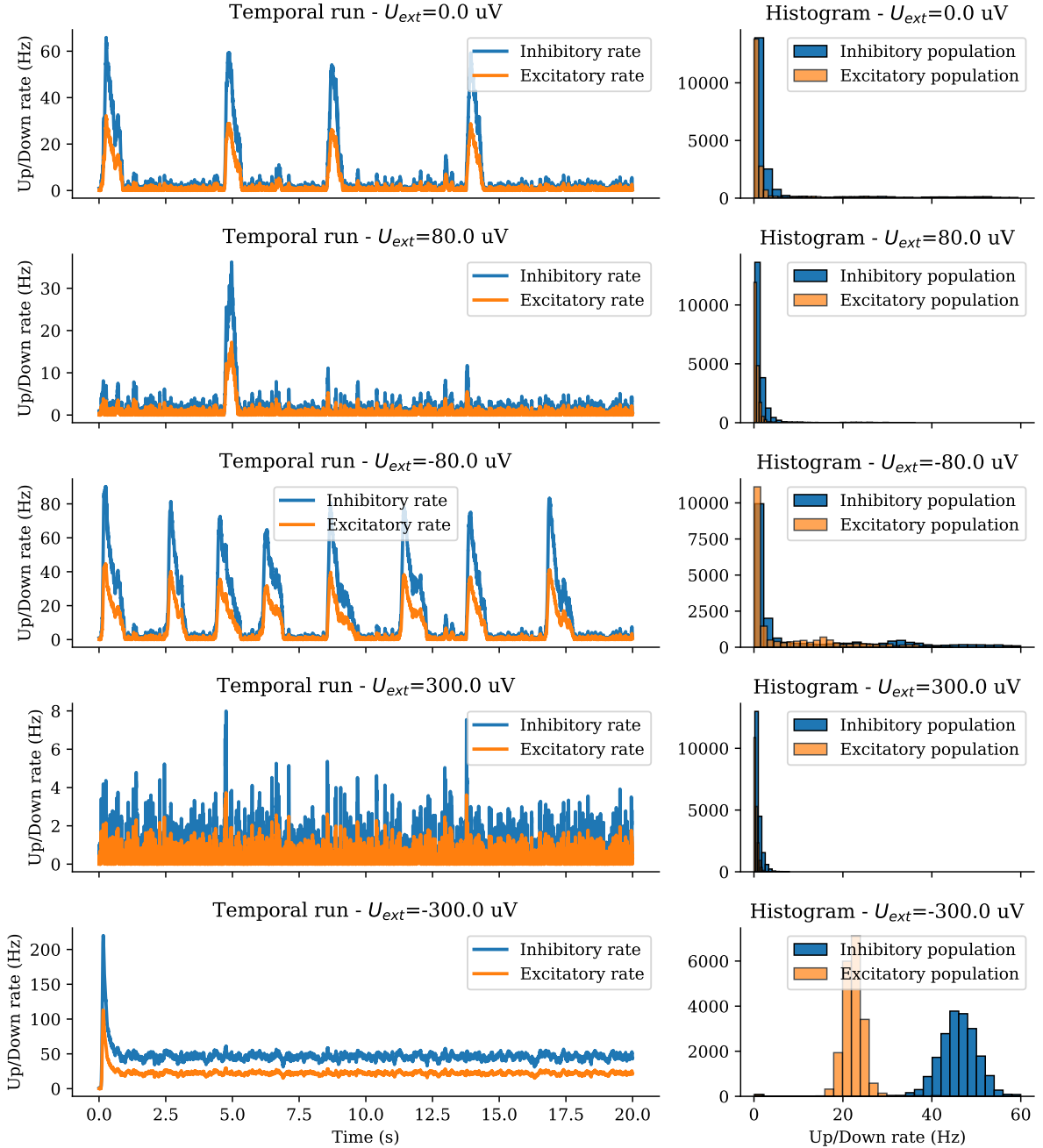


Figure 9: Temporal runs and histogram for constant $U_{ext} \{0.0, 80.0, -80.0, 300.0, -300.0 \mu\text{V}\}$. The different states, SO, AI and depressed, as well as transitions in between the states can be seen in the plots.

6.3 Adaptation study

Following the study of the single mean field model, we turned the attention to analysing the response of the adaptation (τ_{adapt}) in the model. Since the adaptation coefficient is added to the model to provide the On/Off behaviour, a higher adaptation should provide the ability of having stronger/faster synchronisation, and the reverse behaviour is expected with a lower adaptation.

In this experiment we ran the model with different adaptations and external EF to see how the frequency response changed based on the adaptations. See figure 10 for the plot.

The frequency response is similar in all the cases but with a shift of the left part of the frequency response, the higher the adaptation the more shifted to the left. Taking into account that on the left of the frequency response shape the mean field in AI state and in the right is in a depressed state, **by using EFs close to the transition point we can shift the brain tissue from one state to the other.**

With the different betas the same behaviour is maintained, to the left of the frequency response shape the mean field is in AI state, to the right is in depressed state and the shape itself is the synchronised slow oscillations.

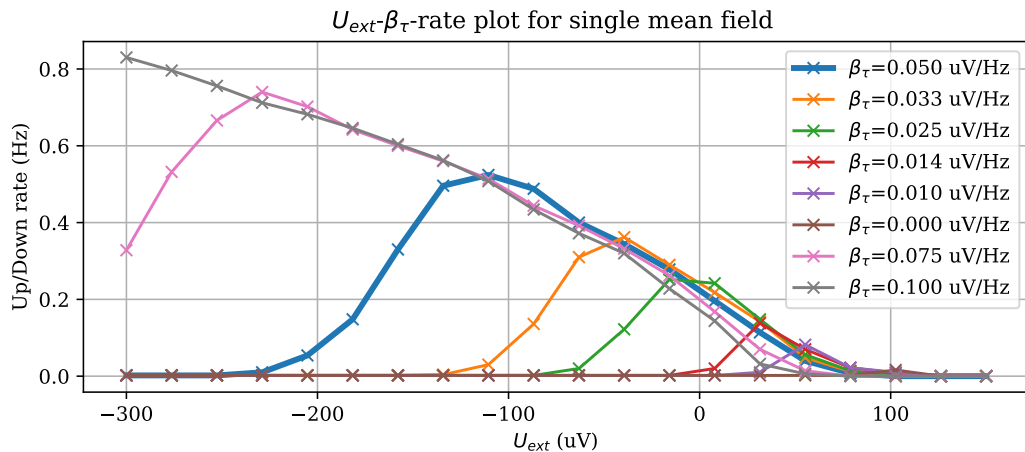


Figure 10: Slow oscillations (SO) frequency for different adaptation coefficients (β_τ). The bigger the β_τ the larger the SO U_{ext} range of values.

6.4 Changing external current U_{ext}

In figure 11 we can see two simulations with On/Off exogenous EF, with conditions close to the transition point so we can see how thanks to the EF the mean field changes state.

In the first run, we have a $150 \mu V$ U_{ext} and the adaptation (β_{adapt}) it is at the estimated value of $0.05 \mu V$, with these parameters we have complete depression when having the U_{ext} activated and synchronised state (0.25 Hz) when the EF is off.

The second run, we have a $45 \mu V$ external EF and a reduced adaptation value of $0.014 \mu V$. While this is not the physiological value of the brain tissue adaptation can be reduced in vitro with a combination of chemicals. In this scenario we have the very interesting **switch from AI state to synchronised state** on the activation of the EF.

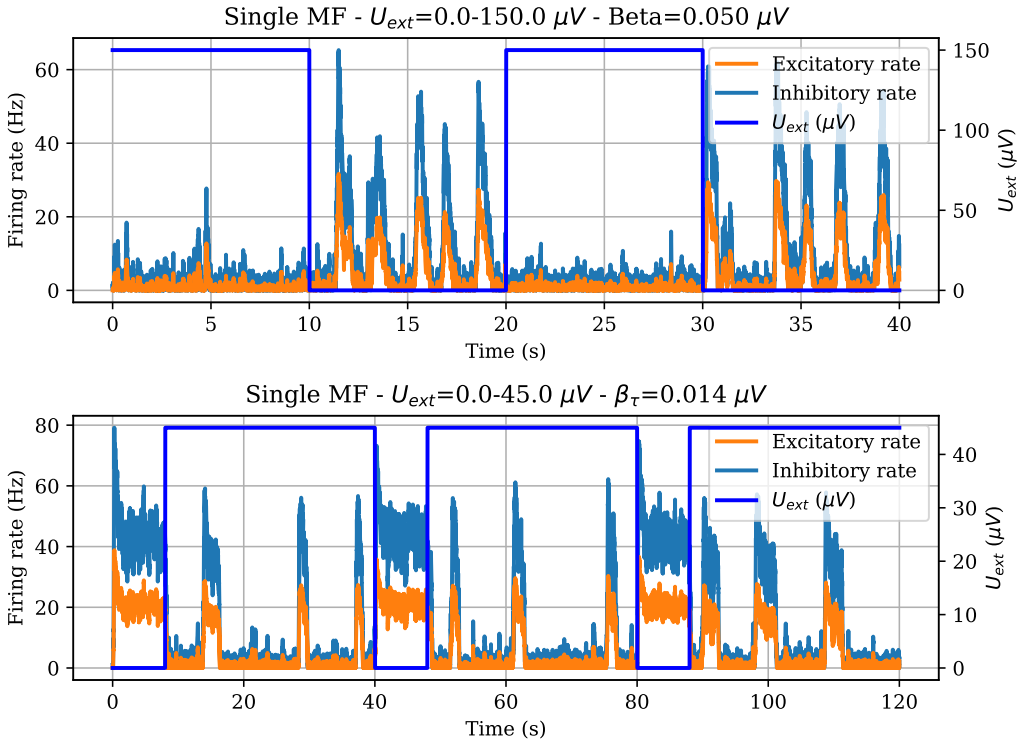


Figure 11: Single mean field model simulations with On/Off constant U_{ext} with 150 μV amplitude and 0.050 μV adaptation (β_τ) in the top plot and 45.0 μV amplitude and 0.014 μV adaptation in the bottom plot.

6.5 Oscillating U_{ext}

The next analysis was to run the single mean field simulations with a non-constant EF. The hypothesis was that there could be some resonance frequency where the model would respond with faster Up/Down oscillations. We tried three scenarios, the first is a standard sinusoidal signal, the second is a positive shifted (positive $A/2$) and the third is negative shifted (negative $A/2$).

See figure 12 for the results. The conclusion from seeing the 3 plots is that the bottom second row consistently has higher On/Off frequencies, suggesting that **there is a range of frequencies that are optimal for any amplitude**. To further study the response to sinusoidal EFs we ran a simulation with a finer range of frequencies and a fixed amplitude, see figure 13. In this experiment we can see that **the optimal frequency is around 1-2 Hz**.

6.6 Two (ephaptically) coupled populations

The next set of experiments focuses on studying the coupling behaviour in a simple setting of two coupled populations. Although in this project we are not interested in the coupling between different populations (since the focus is in external EFs), this analysis proves useful in understanding how the ephaptic coupling fares when co-existing with a constant EF.

In figure 14 we can see some temporal runs of two coupled populations with different parameters.

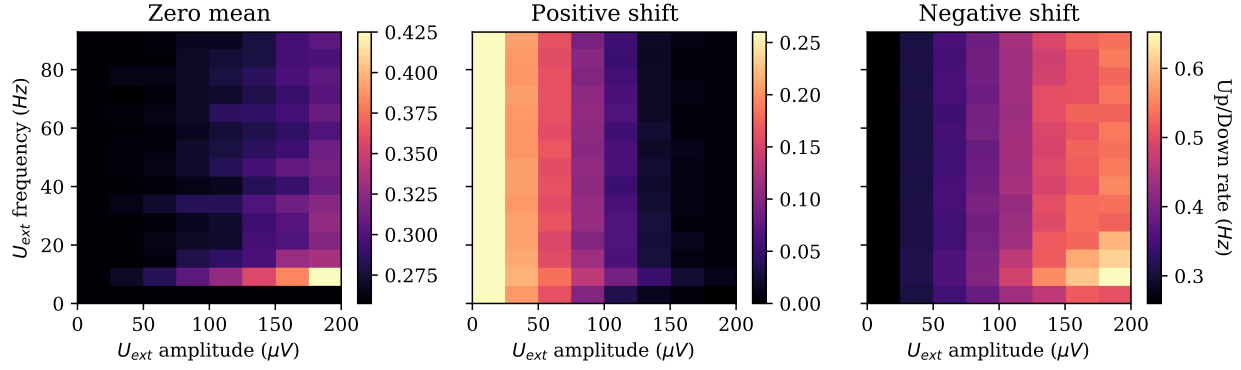


Figure 12: On/Off frequencies for sinusoidal U_{external} with different frequencies and amplitudes. Function for the first plot is $f(t) = A \sin(t * \frac{2\pi}{f})$, second plot $f(t) = A \sin(t * \frac{2\pi}{f}) + A/2$ and third plot $f(t) = A \sin(t * \frac{2\pi}{f}) - A/2$

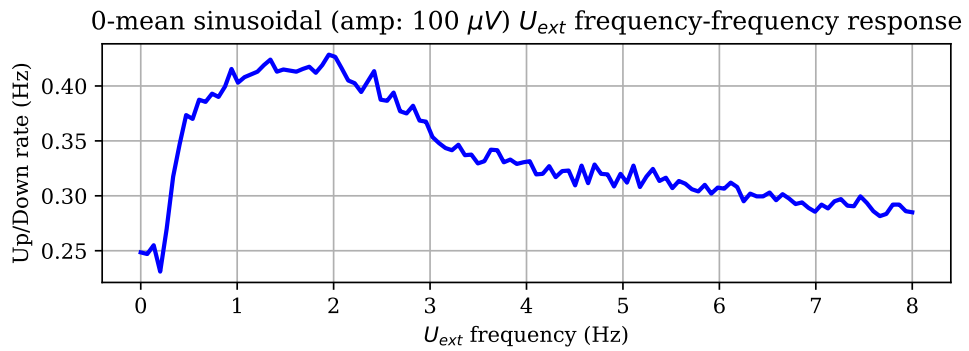


Figure 13: Oscillation frequency - Sinusoidal frequency response curve for a single mean-field model

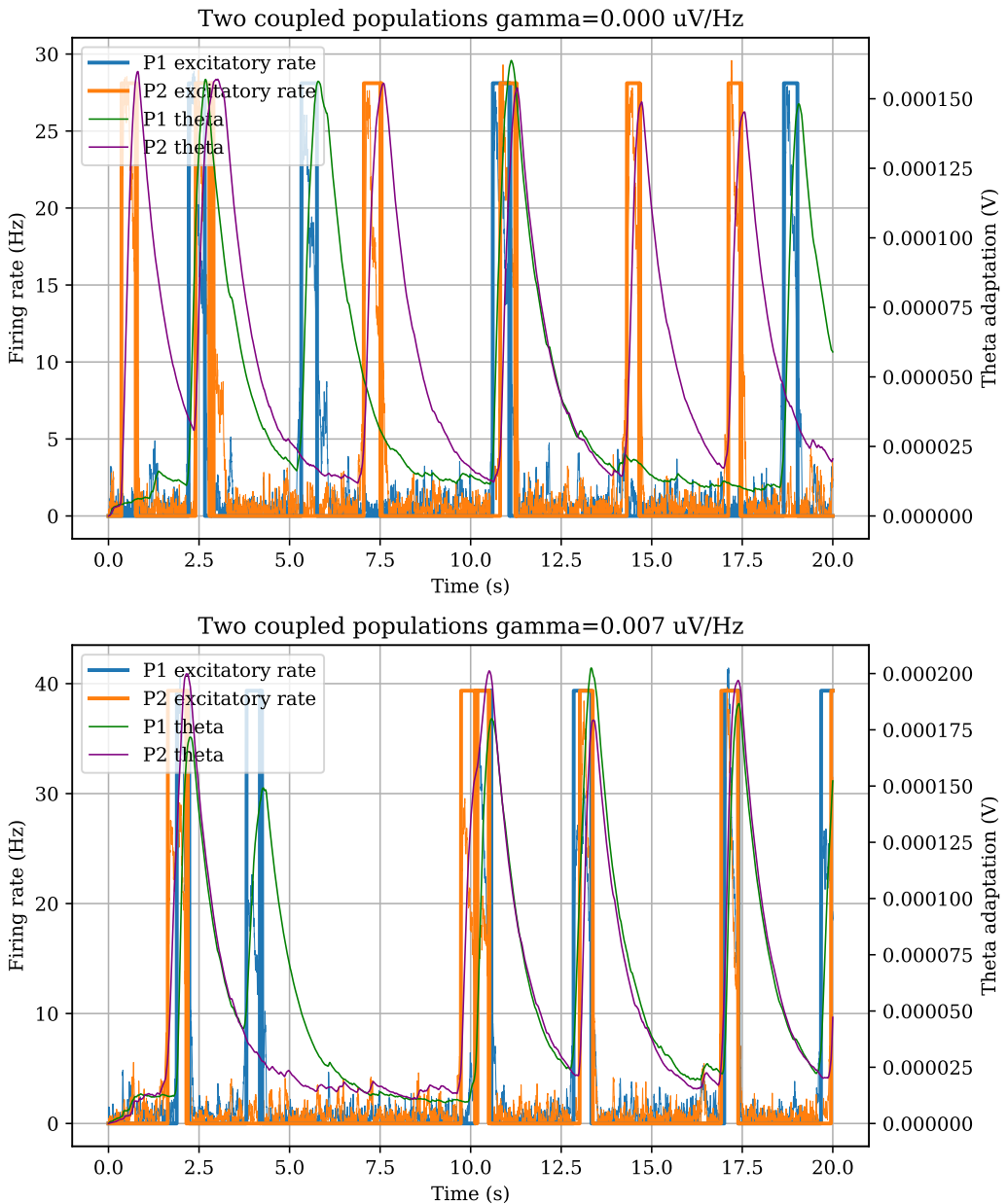


Figure 14: Detailed plot with both populations and adaptation (β_τ) of two coupled populations with different random seed and ephaptic coupling coefficient (γ_{ephaptic}).

6.7 Coupling coefficient study on two populations

To quantify the impact of the coupling coefficient on the model, we ran experiments with an array of coupling coefficients and measured both the frequency and the similarity of the signals.

To measure the similarity between two signals the paper by Rebollo *et al.* [31] uses the phase locking index (PLI) metric. This metric measures the similarity of oscillatory phases. First it low-pass-filters the firing rates of excitatory populations at both sides. And from the band-limited traces it estimates the instantaneous phases of the Up/Down oscillations on both sides using the Hilbert transform. We compute the difference between the phases and quantifies the spread by means of the mean vector length.

$$PLI = \left| \frac{1}{N} \sum_{i=0}^N \exp -i[\phi_L(t_i) - \phi_R(t_i)] \right| \quad (54)$$

The results are on figure 15. There is a positive correlation between the On/Off frequencies of the population models and the coupling coefficients. There is a strong positive correlation with both correlation and PLI and the coupling coefficient, as it can be seen in the second plot of the figure.

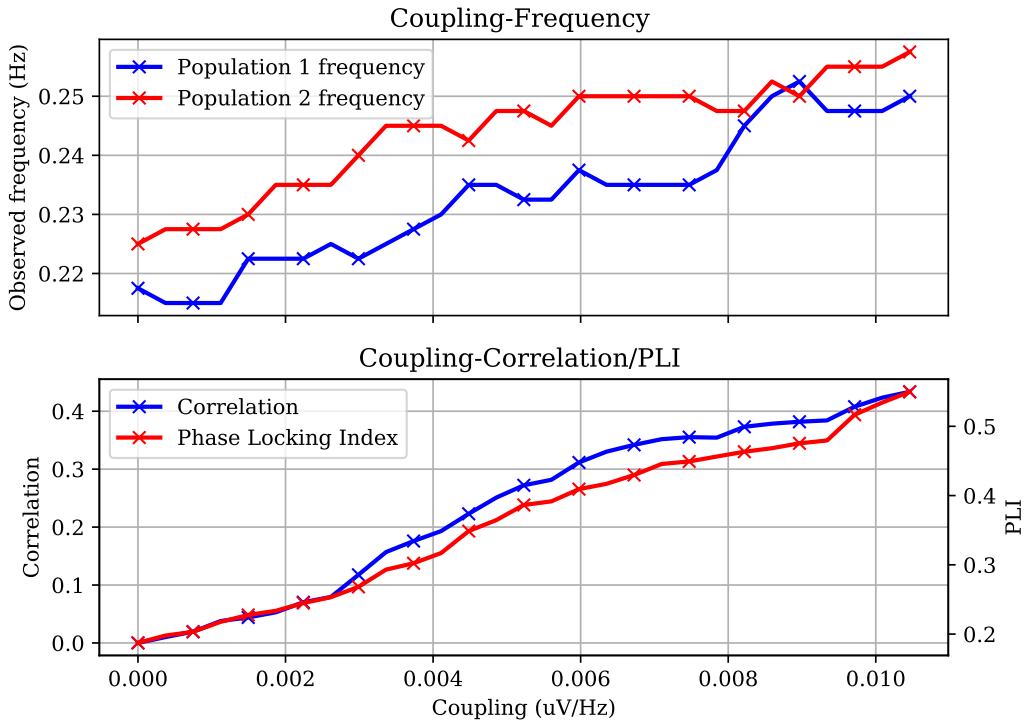


Figure 15: Frequency response to different couplings and Correlation/PLI response to different couplings. It shows a linear relationship between both the populations frequencies, the signals correlation and the PLI to the coupling coefficient.

6.8 Two coupled populations with exogenous current (U_{ext})

The last analysis performed with the two population models was about understanding the impact of a constant EF with the ephaptic coupling. In figure 16 we can see the On/Off frequency and the PLIs for several coupling coefficients on the y-axis and the EF amplitude on the x-axis. It is worth to note that the frequency response is indistinct to the different coupling coefficients, the curve is almost identical to 8. But for the PLIs it has a bigger impact we can see that for values around the $-75 \mu V$ mark there is a large difference, from 0.2 to 0.65 depending on the coupling coefficients. Looking at the larger picture it looks like the higher the frequencies the biggest dispersion that there is on the PLI and the more it the coupling coefficient matters, but when there are low frequencies there is little room for variability.

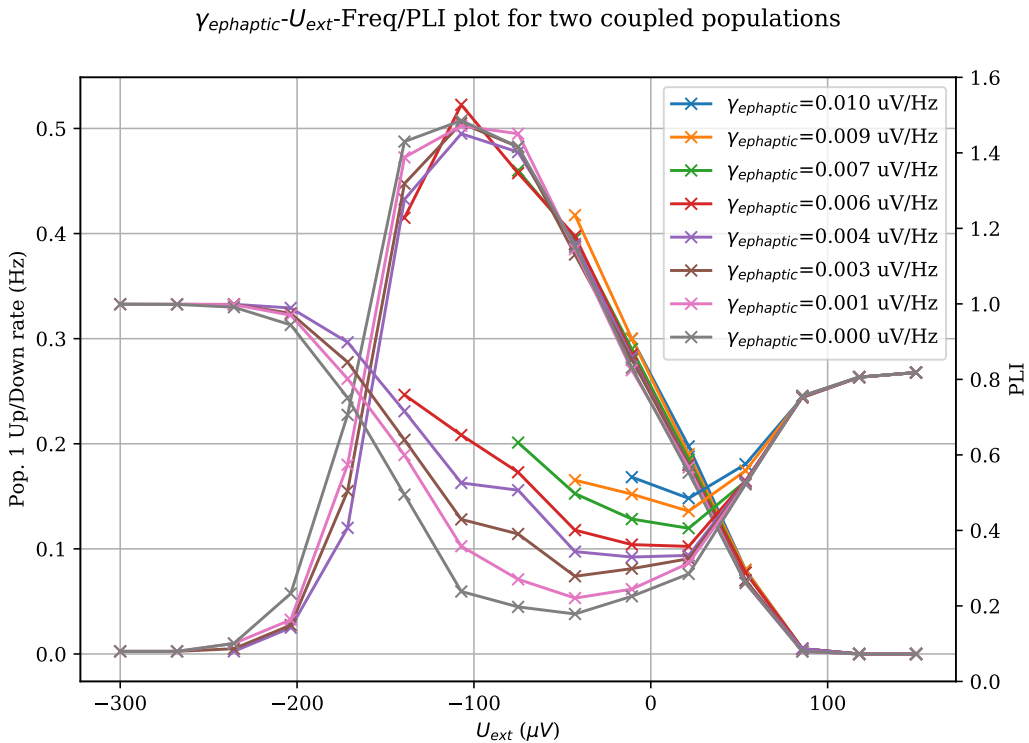


Figure 16: Frequency/PLI response for two coupled mean fields to different external constant EFs (U_{ext}).

7. Data analysis and fitting the model

One of the objectives of the internship was to further develop the model to be able to model the behaviour of exogenous EFs. During the time I was there the objective shifted slightly according to the lab necessities and it ended being with an analysis/extension of the model to be able to represent the synchronisation modulation caused by a rotated EF.

7.1 Data analysis

In the Systems Neuroscience lab at IDIBAPS (Sanchez-Vives *et al.*) they work extensively with *in vitro* measurements of brain tissue. For this project they performed experiments using cortical slices of brain tissue with an externally applied DC current using electrodes. The measurements were done with the electrodes at several angles in respect to the brain tissue, and the recording technique was equivalent to what is explained in section 4.2.

The measurements obtained from a micro electrode array (MEA) are 16 channel recordings of the brain tissue which represent the local field potential (LFP), see a sample of a recording in Figure 17. The goal is to obtain the frequencies, down times and up times from the measurements to then use the model to reproduce the parameters. Some signal processing was done in order to estimate the multi unit activity (MUA) from the LFP, as described in [42][46].

First the LFP recordings were de-meaned to eliminate super-slow oscillations by subtracting the moving average (window length 1s). The MUA was estimated as the power in the Fourier components at high frequencies (>200 Hz) of the extracellular recordings. High frequency components of the extracellular recording can be seen as a linear transform of the instantaneous firing rate of the neurons surrounding the electrode (LFP). The power spectra of the extracellular are computed in 5ms bins. The MUA is the average power of the normalised spectra in the frequency band 0.2-1.5 kHz. Afterwards, the logarithm is applied to the MUAs to balance large fluctuations of the nearby spikes. Furthermore they are smoothed using a moving average filter with a window of 80ms. Finally for each recording the filtered log(MUA) was shifted so that the minimum value was at zero. See Figure 18 for a graphical representation.

Algorithm 2: MUA signal processing

Result: Up period, Down period and frequency

signals = Load the signals from the .smr files;

for each channel do

```
demean_signal = channel - mov_avg; /* 1 second moving average window */
```

for each 5ms window do

```
fft_signal = fft(5mswindow);
```

r

end

`log_mua = log(mua);`

```
/* 1 second moving average window */
```

```
log_mua_ma = mov_avg(log_mua);
```

/* In the 200-1500 Hz band */

```
up_period,down_period,frequency = compute_statistics(log_mua_ma);
```

100

To detect the Up Down states by setting a threshold value on the log(MUA), with some time thresholds

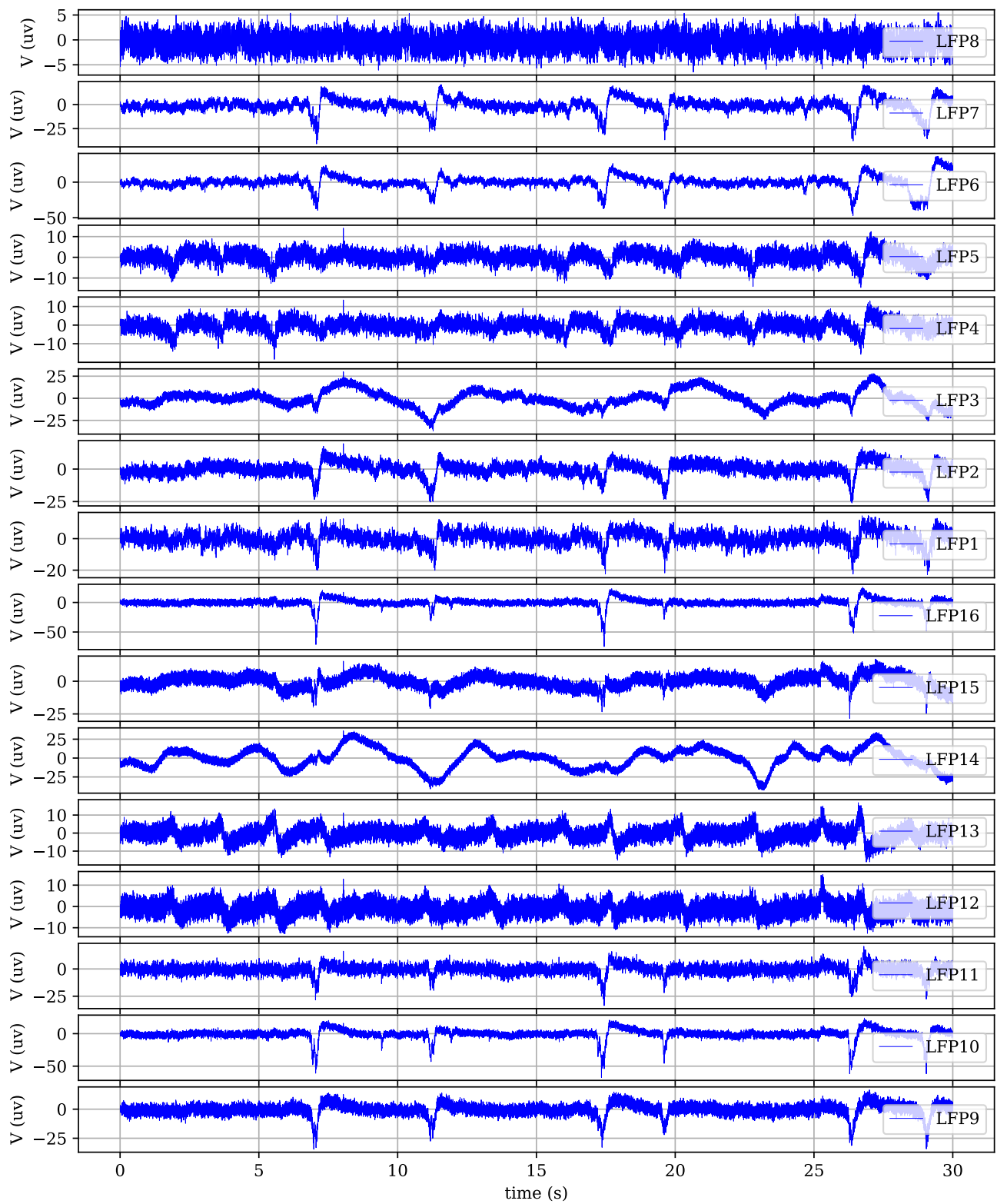


Figure 17: Zoom plot [0s,30s] of a control recording, without any DC field. The signals have been low-pass filtered with a Butterworth filter at a cut-off frequency of 150 Hz.

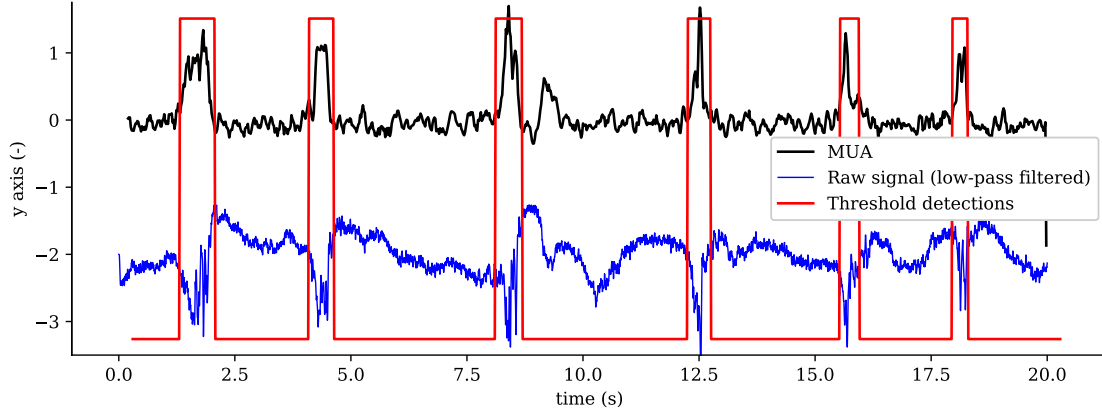


Figure 18: Zoom plot of the raw signal LFP and the computed MUA, using algorithm 2. The raw signal is a particularly good recording of 3 V/m EF with 0 degree orientation (max stimulation). Both signals have been low-pass filtered, scaled and shifted for improved visualisation.

as well. The time durations of the Up and Down states were computed as well, between the time during the events (down to up change and up to down change). The frequency of the slow oscillation SO represents a whole cycle, Up time plus Down time.

We also used an alternative method to get the statistics which involved in directly analysing the LFP recordings. This method was used to analyse some signals which were quite noisy and it performed better than the previous method in this signals. It consists on computing a moving variance filter, which is computing the variance of the signal over a moving window and then using the same threshold method. See figure 19 for an example of this method.

Algorithm 3: LFP signal processing

```

Result: Up period, Down period and frequency
signals = Load the signals from the .smr files;
for each channel do
    demean_signal = channel - mov_avg;           /* 1 second moving average window */
    mv_signal = moving_variance(demean_signal);   /* 50 ms time window */
    up_period,down_period,frequency = compute_statistics(mv_signal);
end

```

Once all the data has been processed and we have obtained the down period, up period and the frequency for each recording, the "best" results are averaged and plotted on figure 20. The best results are the recordings which have less noise and that the up states are more prominent and easier to determine using the threshold method.

The results are coherent with what is expected, assuming the dipole theory on which the publication and the model builds on. When the electrodes are parallel (0 degrees) to the brain tissue orientation the sensibility, and thus the modulation, to the EF is maximal. And when it is at 90 degrees the impact is minimal. This is represented for the down duration and the frequency, when recording the data at 90 degrees the measurement it is roughly the same for all the EFs, and with 0 degrees the modulation is maximal.

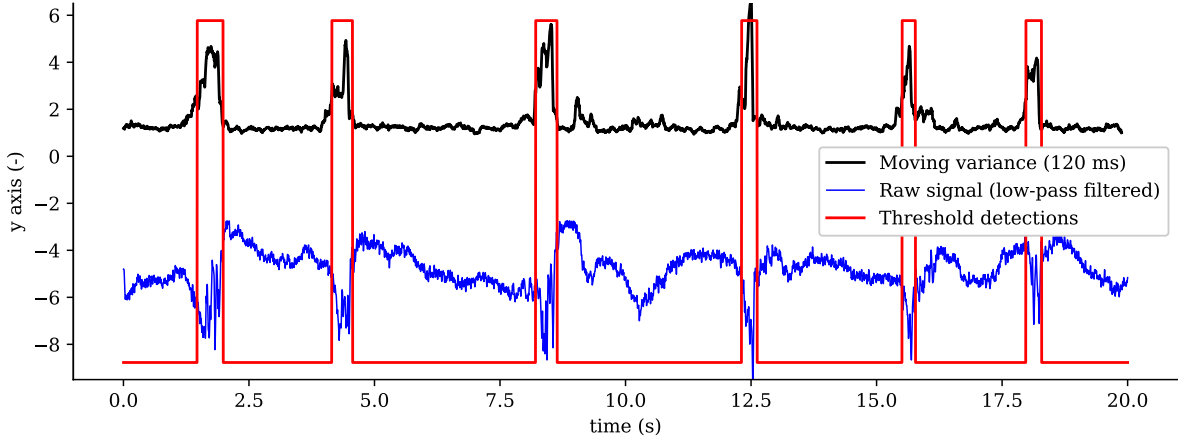


Figure 19: Zoom plot of the raw signal LFP and the computed MUA, using algorithm 3. The raw signal is the same as in 18. Both signals have been low-pass filtered, scaled and shifted for improved visualisation.

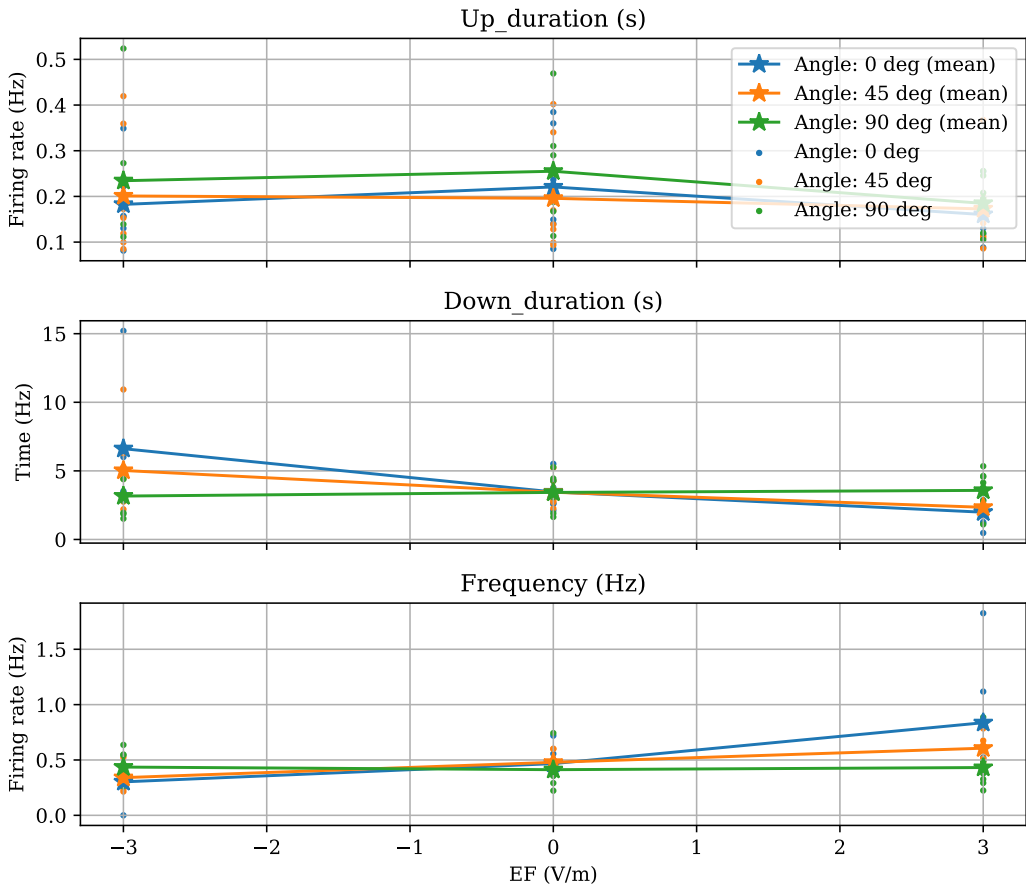


Figure 20: Plot of the up period, down period and the frequency for each experiment and the mean of all of them for each orientation (0,45,90). See values in appendix B.

7.2 Fitting the model to the data

In the previous section we have seen the first phase of fitting the model which consists in processing the data and computing the metrics of interest, up period, down period and frequency. Now we are going to adjust the model to reproduce the computed results. In a similar fashion as we have done in the numerical simulations of the model here we will run some parametric analysis to see how it responds and then will choose the best set of parameters and study the results.

7.2.1 The adaptation equation

The main driver of the Up/Down frequency, and thus of the Up and Down periods as well, is the adaptation equation. Repeated here for clarity,

$$\tau_{adapt} \frac{dU_{adapt}}{dt} = -U_{adapt} + \beta_\tau v_{exc} \quad (55)$$

where τ_{adapt} is the time constant of the ODE, a higher τ_{adapt} causes the adaptation equation to move slower and thus causing longer periods. The β_τ defines the response to the excitatory rate (v_{exc}), so higher β_τ higher frequencies (lower periods). The hypothesis is that with the interplay of these two parameters it will be enough to fit the model to the set of data.

Remember that while the EF, which in turn generates a U_{ext} , doesn't directly impact the adaptation equation, it shifts the threshold in the transfer function and causes a higher mean membrane potential which in turn gives us higher rates and drives the adaptation faster. So the values that we have to run the simulation over is τ_{adapt} , β_τ and U_{ext} . In the Figure 21 there is a selection of some of the results from the $\tau_{adapt} - \beta_\tau - U_{ext}$ simulations.

7.2.2 Noise frequency modulation

Another candidate for the tackling the frequency, down period, up period modulation is the excitation noise. While it is not obvious how the noise affects the dynamics of the up/down oscillation, the experiments have a conducive conclusion.

The main mechanism of modulation is the following, the excitation noise impacts both the excitatory population and the inhibitory one, and by doing that it generates extra activity that impacts the final oscillatory behaviour since the oscillations are proportional to the activity. In figure 22 there are the frequency results for an array of noise and membrane potential shifts.

The conclusion is that the excitation noise has a strong modulation on the frequency. But we are not going to explore the excitation noise as another parameter since the $(\tau_{adapt}, \beta_\tau)$ set is already good enough to reproduce qualitatively and quantitatively the results. In order to have a more realistic model the noise could be quantified at the experimental level, then incorporate that measure in the model and perform the same parameter search using the excitation noise constant.

7.2.3 Parameter search algorithm

Finding the optimal set of parameters for the $(\tau_{adapt}, \beta_\tau)$ happened to be a problem in itself, while in a 2d parameter space is relatively easy to figure your way around and understand what is going on, in the 3 dimensional space this is not trivial. To solve this problem we implemented a simple search algorithm to find the best set of parameters (out of the set of simulations) for the averaged data.

We assumed the hypothesis that the EF impacts the membrane potential based on the cosinus of the

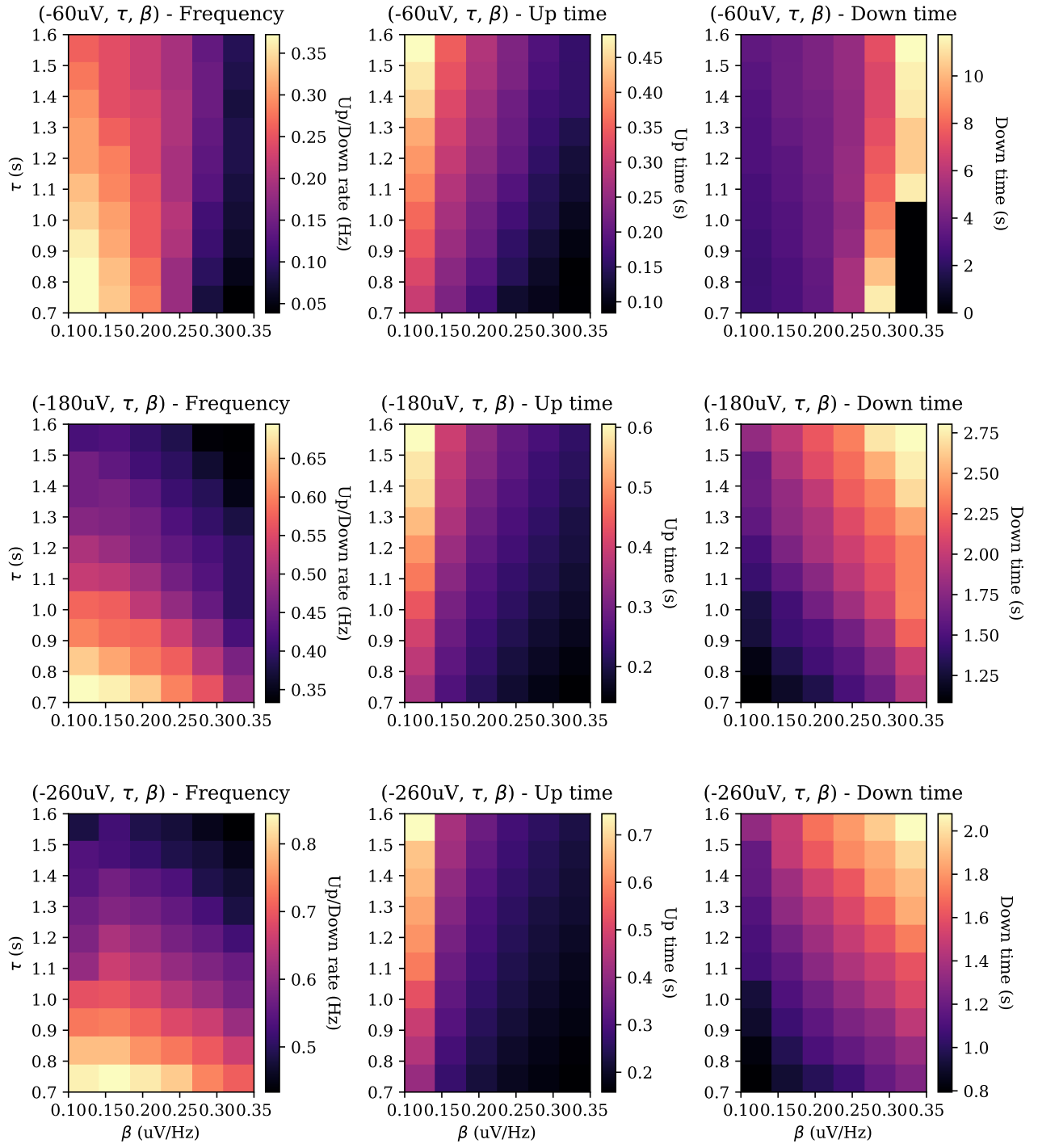


Figure 21: Up/Down frequency, down time and up time plots for a matrix of $(\tau_{adapt}, \beta_\tau)$ and selected U_{ext} {-60 μ V,-180 μ V,-260 μ V} plots. Take note of the inherent complexity of finding a set of parameters that fit the data recordings.

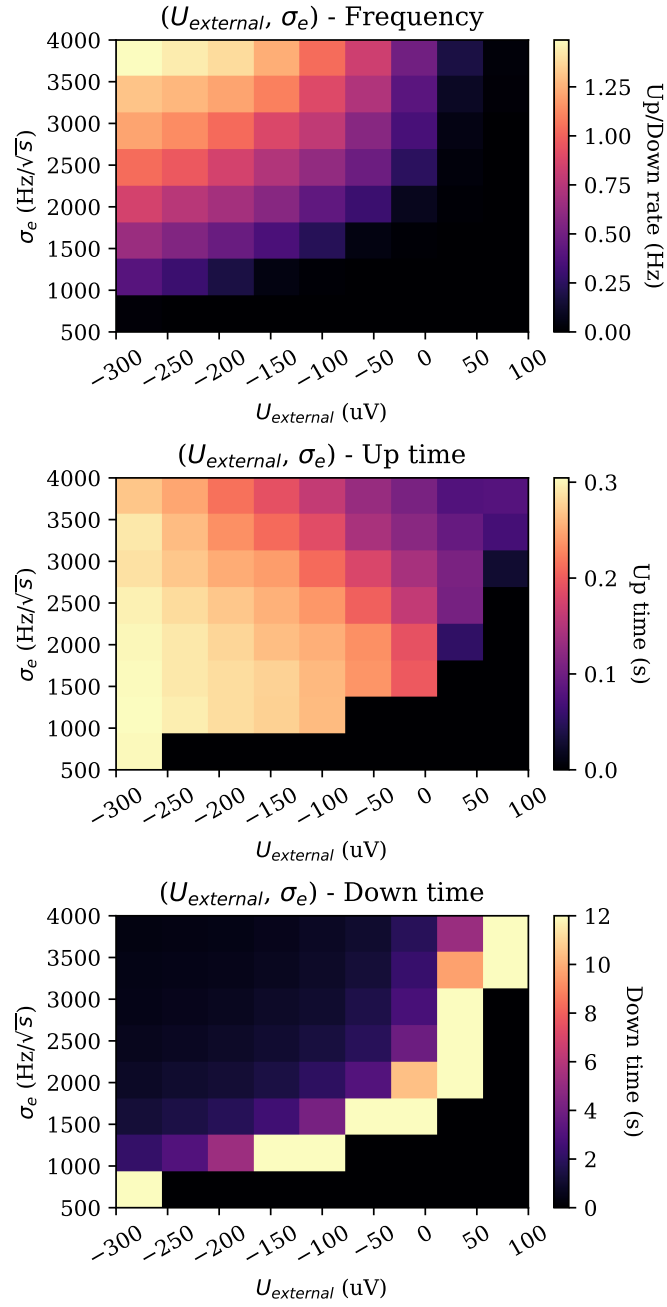


Figure 22: Up/Down frequency plots for a matrix of $(U_{\text{external}}, \sigma_e)$. We can see that the response takes a radial shape from the top left corner for the frequency and down time plot, and from the left side for the up time.

angle, then by reproducing the 0 case we can also reproduce the other recordings, and in fact extrapolate the results to a range of rotations. So, the parameter set optimisation is constrained to the 0 degree case.

Some peculiarities of the present problem is that it needs to optimise the data through the three objective metrics, frequency, down period and up period. Second, is that for the three metrics we have three electric field measurements, so this means selecting three combinations of U_{ext} values to measure the fit to the data. A direct consequence from the last characteristic is that the parameter selection may not have a linear U_{ext} response to the parameters, i.e. the parameters fits the 0 V/m EF for a U_{ext} of -80 μ V, then the 3V/m EF fits it for -40 μ V and finally the -3 V/m fits it for -200 μ V, meaning that the U_{ext} response is not linear and we would need a transformation on top of the model to convert the EF to membrane voltage.

For each parameter set, $\Omega = (U_{ext}, \tau_{adapt}, \beta_\tau)$, it computes a loss metric for each of the voltages $\{-3, 0, 3\}$ V/m. The metric is a weighted squared loss:

$$Loss_\Omega^{EF} = w_{freq}(freq_\Omega - freq_{measured})^2 + w_{down}(down_\Omega - down_{measured})^2 + w_{up}(up_\Omega - up_{measured})^2 \quad (56)$$

The choice of the weights of the loss could be an optimisation problem by itself, luckily we didn't go that way and just used it to run experiments manually. Extra detail is given at a later point.

Next step is to compute the loss metric over the three different electric fields. This means computing the sum of the loss over the 3-combination set of all the U_{ext} parameters, with $n * (n - 1) * (n - 2)$ parameters with n being the number of different U_{ext} . The loss of the optimal combination (lowest loss) is picked and assigned to that specific set of parameters, then the (tau,beta) parameter set are sorted and the best parameter sets are selected for further studies.

The selection of just the lowest loss is a greedy step in the algorithm, although it simplifies the computations it throws away useful information, i.e. if a specific parameter set Ω ranks high for **different combinations** of U_{ext} it means that it may generalise better. We considered adding an extra step weighing the different positions of the 3-combinations of U_{ext} for every parameter step to have an extra dimension, but after some thought we threw away the idea and maintained the greedy step of just picking the best loss.

Algorithm 4: Parameter search algorithm

```

Result: Sorted  $(\tau_{adapt}, \beta_\tau)$  parameters by a custom loss
simulations = Load the results from the  $(U_{ext}, \tau_{adapt}, \beta_\tau)$  simulations;
simulations_0 = Select only the angle 0; /* Optimising over only one scenario */
for each  $(U_{ext}, \tau_{adapt}, \beta_\tau)$  do
    for each recorded EF (-3,0,3) do
        | loss = compute custom loss;
    end
end
for each  $(\tau_{adapt}, \beta_\tau)$  do
    for each combination of EF losses do
        | losses = sum of the loss combination;
    end
    min_loss = pick smallest loss and assign it to the current  $(\tau_{adapt}, \beta_\tau)$  set;
end
sorted_params = sort  $(\tau_{adapt}, \beta_\tau)$  according to min_loss;
```

7.2.3 A problem in the data analysis

During model fitting, we found a roadblock when trying to simultaneously fit the down period, the up period and the frequency to the recordings. It was very difficult to get a good fit and the loss metrics were always high. The problem became obvious after running plots of the averaged periods and frequency from the recordings and realising that the averaged frequencies were always larger than the frequencies computed as the inverse of the sum of the periods ($1/(up+down)$). In figure 26 this is shown in a graphical format.

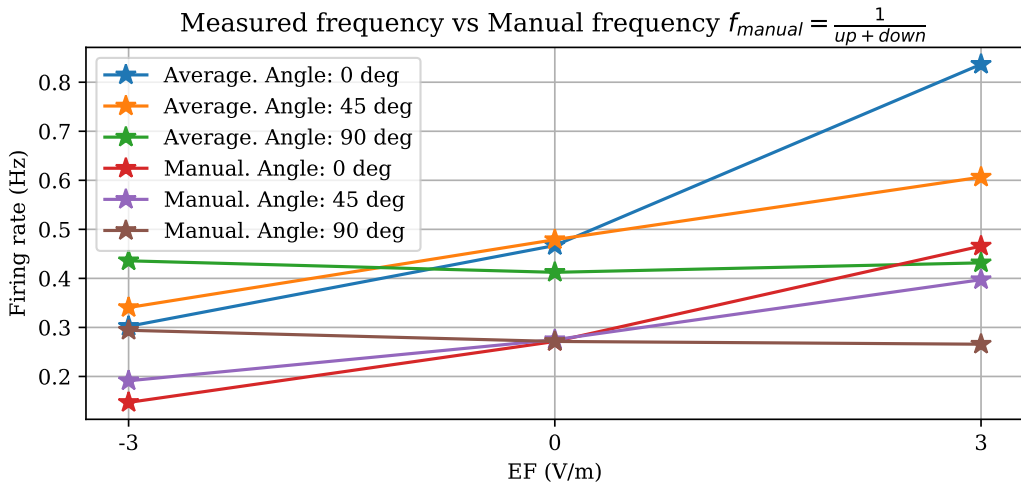


Figure 23: Averaged frequency measurements ($E(frequencies)$) and manual frequency ($1/E(periods)$) with averaged period measurements. Notice how the manual frequency has significantly lower frequencies when compared with the averaged frequency measurements.

The problem comes from the inequality between the mean of periods and the mean of rates, which is the inverse of the period. Since expectation is not a linear operator the averaging is not correct. The harmonic mean should be considered when dealing with averaging over rates. This is known as the HM-AM inequality

$$\frac{1}{n} \sum_{i=1}^n x_i \leq \frac{n}{\sum_{i=1}^n 1/x_i} \quad (57)$$

7.2.4 Putting everything together

Let's not forget what the main goal of the chapter is, to adapt the model to reproduce the modulation of rotated EFs. So far we have seen how to fit the computer model simulations to the recordings, with the parameter search algorithm. But still we have just fitted the model across the y-axis, the Up/Down frequency.

The next step is to fit the x-axis, to do so we assumed two hypothesis. First, an external EF produces a membrane potential shift with a linear relationship, a constant $\gamma_{external}$ is added for the relation. Second, a rotated EF produces a membrane potential shift proportional to the cosinus. So the membrane potential shift $U_{external}$ is modelled as,

$$U_{external} = \gamma_{external} * EF * \cos(angle). \quad (58)$$

Another option for the x-axis was to model it as a non-linear relationship, $f_{EF}(EF)$. Since the parameter search algorithm optimises through the whole set of combinations of the U_{external} values, it was possible that a good fit was only possible with a non-linear relation. But after running some experiments we found that the fit was good with a linear relation.

7.2.5 The results

The final measurements were obtained by running two parameter grid simulations, the first with a wide array of values and the second with a finer resolution focusing on the set of parameters from the first simulation with better fit. See figure 24 and 25 for the values used in each simulation.

$$\begin{aligned} U_{\text{ext}} &: \{-200, -150, -75, 0, 75, 115, 150, 200\} \mu V \\ \tau_{\text{adapt}} &: \{200, 250, 300, 350, 400, 800, 1200, 1600\} \text{ ms} \\ \beta_{\tau} &: \{0.05, 0.1, 0.15, 0.2, 0.25, 0.3, 0.35\} \mu V/\text{Hz} \end{aligned}$$

Figure 24: Values used for the first parameter grid simulation. For every parameter set $\Omega = \{U_{\text{ext}}, \tau_{\text{adapt}}, \beta_{\tau}\}$ the up period, the down period and the frequency was computed.

$$\begin{aligned} U_{\text{ext}} &: \{-380, -340, -300, -260, -220, -180, -140, -100, -60, -20\} \mu V \\ \tau_{\text{adapt}} &: \{700, 800, 900, 1000, 1100, 1200, 1300, 1400, 1500, 1600\} \text{ ms} \\ \beta_{\tau} &: \{0.50, 0.1, 0.15, 0.2, 0.25, 0.3, 0.35\} \mu V/\text{Hz} \end{aligned}$$

Figure 25: Finer selection of values used in the second parameter grid simulation. Like in the first simulation the up period, the down period and the frequency was computed for every parameter set $\Omega = \{U_{\text{ext}}, \tau_{\text{adapt}}, \beta_{\tau}\}$.

The parameter search algorithm was run on both parameter grid simulations and the results were studied using a variety of loss weights. Since the weights can be custom defined for each run of the parameter search, more importance can be given to the qualitatively more relevant values. In our case, these were the down time and the frequency, since the up time presented noise and the measurement didn't look reliable. See Figure 26 for the up period, down period and frequency measurements for the top 4 parameter sets. In Appendix C the top 20 parameter sets can be found.

As of now, just the y-axis values (up period, down period, frequency) have been fitted. The next step was to fit the simulation values to the x-axis. As explained in section 7.2, the U_{ext} can be modelled from the EF with the following equation

$$U_{\text{external}} = \gamma_{\text{external}} * EF * \cos(\text{angle}). \quad (59)$$

Since we have just three EF measurements, we were able to run a simple procedure manually until a qualitative good fit was found. First, select the x-axis (U_{ext}) shift to get a value of the model simulation to match the 0 V/m EF value. The shift value is added to the excitation threshold, since it is equivalent to having a constant U_{ext} , see eq. 46. The new excitation threshold is

$$\theta_e^{\text{new}} = \theta_e^{\text{old}} + \text{shift} \quad (60)$$

Then under the assumption that the U_{ext} -frequency relationship is linear, we can select the x-axis jump to the left and to the right for the model simulation to fit for the -3 V/m and 3 V/m measurements. Then

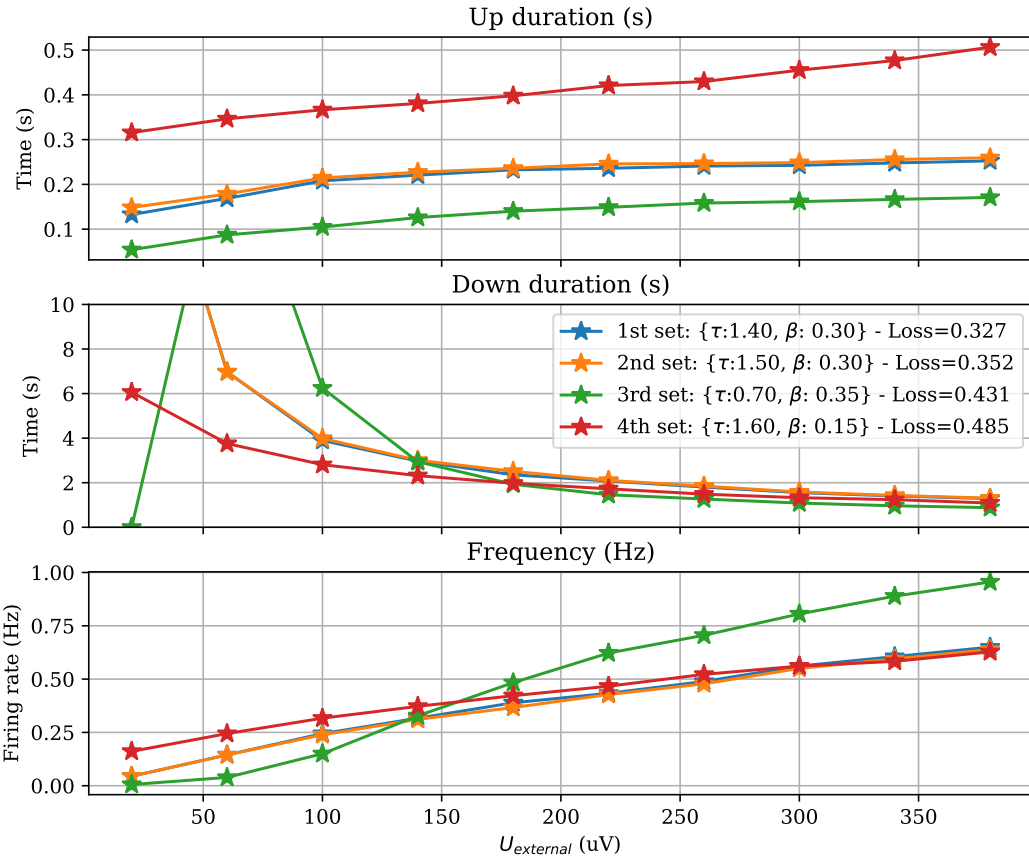


Figure 26: Plot of the 4 best parameter sets $(\tau_{\text{adapt}}, \beta_{\tau})$ metrics, optimised with quadratic loss with weights: $\{w_{\text{down}}: 1, w_{\text{up}}: 1, w_{\text{freq}}: 0\}$, for a range of U_{external} . For table with the full parameter optimisation results see appendix C.

the external gamma coefficient is

$$\gamma_{\text{external}} = \frac{\text{jump}}{3} \quad (61)$$

The parameters selected to fit the data to the rotated EF measurements are $\tau_{\text{adapt}} = 1.4s$, $\beta_{\tau} = 0.3$, $\theta_e = -50.13mv$, $\gamma_{\text{external}} = 80/3$. See figure 27 for a plot of the fitted results.

To further improve the fitting of the values we could have coded a *shift* and *jump* optimisation step inside the parameter loss, so the parameter search algorithm would do a global search rather than a constrained parameter search. But for the given situation, the improvement would be marginal, the results are already close enough. The end goal of the model fitting is to see if the model can in fact represent the qualitative behaviour of the recordings rather than an exact representation of values, and in this case we achieve a reproduction of the behaviour and a good fit to the existing data.

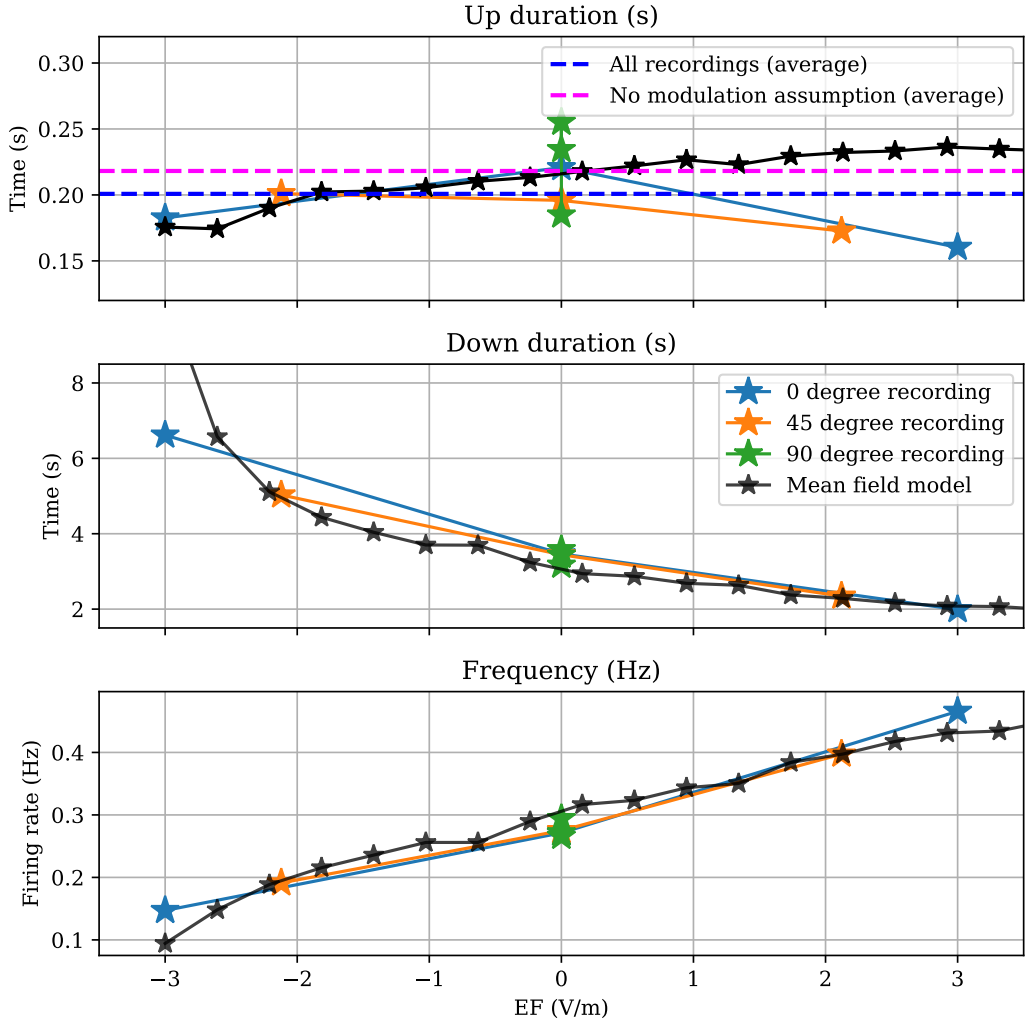


Figure 27: Up period, down period and frequency values for both the mean field simulation and the EF recordings, after adjusting the model with the best parameter set ($\tau_{adapt} = 1.4s$, $\beta_\tau = 0.3\mu V/Hz$). The up period plot also contains the average of all the measurements, and the average of the non modulating EFs, which are the all the 0 V/m and the 90 degree ± 3 V/m. We see a qualitative good fit for the down duration and the frequency, for the up duration the signal is quite noisy and we discarded the signal for that reason.

8. Conclusions

In this master thesis we have implemented and analysed a mathematical model of the modulation caused by electrical fields on the cerebral cortex activity. It studies the brain activity with endogenous and exogenous electric fields with different intensities and orientations. It also studies the model interaction with network parameters like adaptation, time constants and coupling coefficients. In addition the interaction between different neuronal populations has been studied.

We have observed that for electric fields of larger intensity there is an increase on the Up/Down frequency, also known as slow oscillations, equivalent to slow wave sleep or anaesthesia situations. Still, the model shows that the emergent activity shifts from slow oscillations to asynchronous irregular state with an (even) stronger electric field, simulating what could be the change from sleep to awake. For a negative electric field the model goes to a non-physiological depressed state where the population has very low activity.

Regarding the relation with adaptation (beta), the computer simulations show that the Up/Down frequency response to electric fields changes with different adaptation coefficients, and the threshold for the change of state from slow oscillations to asynchronous irregular is shifted to a larger value, while the change threshold from slow oscillations to depressed state is maintained.

Another result from the project is the study of the model under a oscillating (sinusoidal) membrane potential shift. Simulation were performed under the influence of a zero mean signal, a positive mean signal ($A/2$) and a negative mean signal ($-A/2$). The conclusion is that there is an optimal frequency, for the three types of signals, around the 1-2Hz. Further research in this direction could be to study different excitation functions and their impact on the activity response, also to study the temporal aspects of the changes in the brain tissue, i.e. how fast we see activity rise after activating an exogenous electric field, also how the membrane potential polarisation responds to changing electric fields.

To study the interaction between different neuronal populations we focused on the 2 networks scenario, since it is the simplest one, and thus it can help in understanding the relationship between the interactions. The model shows a small positive correlation between the membrane shift potential and the populations frequency, and a large positive correlation between the membrane shift potential and the correlation and PLI metrics.

Some of these results have been validated experimentally. We have been able to adjust the model parameters so that we get a qualitative and quantitative good representation of the experimental recordings. Using a simple parameter search algorithm and manual tuning has been enough to get the results. The inherent simplicity and ease of the parameter search allows to customise it with different weight for each of the objective metrics (up period, down period and frequency in this case), to get further conclusions and really understand how the parameters affect the response.

Given the low resolution of the experimental data, 3 electric field intensities and 3 angles, we can't really say that the current mean-field model is able to completely reproduce the behaviour of the brain tissue. Some extra measurements, with more electric fields and rotation resolution are needed to validate the model. It would be relevant to see if the non-linear response that we see in the model in the left of the x-axis, also happens in the experiments and at which electric field intensity. It would also be interesting check if the hypothesis that the membrane shift potential responds to the cosinus of the angle is true.

Another direction for further study would be the quantification of the noise in the experiments, taking into account both the recording instruments noise and the inherent noise of the brain tissue. With this metric we could use it in the model and then relaunch the parameter grid simulations and parameter search

and get a more representative model.

The limitations of the current mean field approach are the simplicity of the model and the low explainability of the events in the simulations, since in the derivation of the model itself we are removing any redundant information. On a more technical side, a main limitation of the mean-field approach is that it requires on the knowledge of the transfer function of neurons. There are derivations for a number of models, such as integrate-and-fire, AdEx and the Hodgkin-Huxley. However, the transfer function is not easy to define in other cases, such as bursting neurons.

Nonetheless, the model is a good illustration of the importance to quantify, predict and highlight the relevance between the theoretical approximation and the experimental one, since the first one allows to explore aspects which are not always possible to investigate experimentally, therefore models contribute to quantification and mechanistic explanation.

Jaume Colom Hernandez

References

- [1] K. Saladin, *Human anatomy (3rd ed.)*. McGraw-Hill, 2011.
- [2] M. Steriade, A. Nuñez, and F. Amzica, "A novel slow ($\downarrow 1$ Hz) oscillation of neocortical neurons in vivo: depolarizing and hyperpolarizing components," *J Neurosci*, vol. 13, pp. 3252–3265, Aug 1993.
- [3] G. T. Neske, "The slow oscillation in cortical and thalamic networks: Mechanisms and functions," *Frontiers in Neural Circuits*, vol. 9, p. 88, 2016.
- [4] M. V. Sanchez-Vives and D. A. McCormick, "Cellular and network mechanisms of rhythmic recurrent activity in neocortex," *Nat Neurosci*, vol. 3, pp. 1027–1034, Oct 2000.
- [5] P. Berens, G. A. Keliris, A. S. Ecker, N. K. Logothetis, and A. S. Tolias, "Feature selectivity of the gamma-band of the local field potential in primate primary visual cortex," *Front Neurosci*, vol. 2, pp. 199–207, Dec 2008.
- [6] S. Katzner, I. Nauhaus, A. Benucci, V. Bonin, D. L. Ringach, and M. Carandini, "Local origin of field potentials in visual cortex," *Neuron*, vol. 61, pp. 35–41, Jan 2009.
- [7] P. Fries, J. H. Reynolds, A. E. Rorie, and R. Desimone, "Modulation of oscillatory neuronal synchronization by selective visual attention," *Science*, vol. 291, pp. 1560–1563, Feb 2001.
- [8] P. Fries, T. Womelsdorf, R. Oostenveld, and R. Desimone, "The effects of visual stimulation and selective visual attention on rhythmic neuronal synchronization in macaque area V4," *J Neurosci*, vol. 28, pp. 4823–4835, Apr 2008.
- [9] A. Gail, H. J. Brinksmeyer, and R. Eckhorn, "Perception-related modulations of local field potential power and coherence in primary visual cortex of awake monkey during binocular rivalry," *Cereb Cortex*, vol. 14, pp. 300–313, Mar 2004.
- [10] J. Liu and W. T. Newsome, "Local field potential in cortical area MT: stimulus tuning and behavioral correlations," *J Neurosci*, vol. 26, pp. 7779–7790, Jul 2006.
- [11] F. Frohlich and D. A. McCormick, "Endogenous electric fields may guide neocortical network activity," *Neuron*, vol. 67, p. 129–143, 2010.
- [12] C. A. Anastassiou, R. Perin, H. Markram, and C. Koch, "Ephaptic coupling of cortical neurons," *Nat Neuroscience*, vol. 67, p. 129–143, 2010.
- [13] S. A. Weiss and D. S. Faber, "Field effects in the CNS play functional roles," *bioRxiv*, vol. 2018, p. 246819, 2018.
- [14] C. A. Anastassiou and C. Koch, "Ephaptic coupling to endogenous electric field activity: Why bother?," *Curr. Opin. Neurobiology*, vol. 31, pp. 95–103, 2015.
- [15] B. Katz and O. H. Schmitt, "Electric interaction between two adjacent nerve fibres," *J. Physiol.*, vol. 97, pp. 471–488, 1940.
- [16] J. G. Jefferys, "Nonsynaptic modulation of neuronal activity in the brain: electric currents and extracellular ions," *Physiol Rev*, vol. 75, pp. 689–723, Oct 1995.

- [17] M. B. D. Reato, A. Rahman and L. C. Parra, "Low-intensity electrical stimulation affects network dynamics by modulating population rate and spike timing," *J. Neurosci.*, vol. 30, pp. 15067–15079, 2010.
- [18] S. L. Schmidt, A. K. Iyengar, A. A. Foulser, M. R. Boyle, and F. Fröhlich, "Endogenous cortical oscillations constrain neuromodulation by weak electric fields," *Brain Stimul.*, vol. 7, p. 878–889, 2014.
- [19] M. Bikson, M. Inoue, H. Akiyama, J. K. Deans, J. E. Fox, H. Miyakawa, and J. G. Jefferys, "Effects of uniform extracellular DC electric fields on excitability in rat hippocampal slices in vitro," *J Physiol*, vol. 557, pp. 175–190, May 2004.
- [20] J. K. Deans, A. D. Powell, and J. G. Jefferys, "Sensitivity of coherent oscillations in rat hippocampus to AC electric fields," *J Physiol*, vol. 583, pp. 555–565, Sep 2007.
- [21] F. E. Dudek, R. W. Snow, and C. P. Taylor, "Role of electrical interactions in synchronization of epileptiform bursts," *Adv Neurol*, vol. 44, pp. 593–617, 1986.
- [22] M. Steriade, I. Timofeev, and F. Grenier, "Natural waking and sleep states: a view from inside neocortical neurons," *J Neurophysiol*, vol. 85, pp. 1969–1985, May 2001.
- [23] K. L. Hoffman, F. P. Battaglia, K. Harris, J. N. MacLean, L. Marshall, and M. R. Mehta, "The upshot of up states in the neocortex: from slow oscillations to memory formation," *J Neurosci*, vol. 27, pp. 11838–11841, Oct 2007.
- [24] R. Kirov, C. Weiss, H. Siebner, J. B. J., and L. Marshall, "Slow oscillation electrical brain stimulation during waking promotes eeg theta activity and memory encoding," *Proc. Natl. Acad. Sci. USA*, 2009.
- [25] L. Marshall, H. Helgadóttir, M. Mölle, and J. Born, "Boosting slow oscillations during sleep potentiates memory," *Nature*, vol. 444, pp. 610–613, Nov 2006.
- [26] G. Blohm, K. P. Kording, and P. R. Schrater, "A how-to-model guide for neuroscience," *eNeuro*, vol. 7, 2020.
- [27] T. P. Trappenberg, *Fundamentals of Computational Neuroscience*. Oxford Press, 2010.
- [28] A. Destexhe, "Mean-field models of neuronal populations." http://cns.iaf.cnrs-gif.fr/outline_meanfield.html, March 2021.
- [29] A. Salles, J. Bjaalie, K. Evers, M. Farisco, B. Fothergill, M. Guerrero, H. Maslen, J. Muller, T. Prescott, B. Stahl, H. Walter, K. Zilles, and K. Amunts, "The human brain project: responsible brain research for the benefit of society," *Neuron*, vol. 101, pp. 380–384, 2019.
- [30] P. Sanz Leon, S. Knock, M. Woodman, L. Domide, J. Mersmann, A. McIntosh, and V. Jirsa, "The virtual brain: a simulator of primate brain network dynamics," *Frontiers in Neuroinformatics*, vol. 7, p. 10, 2013.
- [31] B. Rebollo, B. Telenczuk, A. Navarro-Guzman, A. Destexhe, and M. V. Sanchez-Vives, "Modulation of intercolumnar synchronization by endogenous electric fields in cerebral cortex," *Science Advances*, vol. 7, no. 10, 2021.

- [32] H. David and T. N. Wiesel, "Effects of monocular deprivation in kittens," *Naunyn-Schmiedebergs Archiv für Experimentelle Pathologie und Pharmakologie* 248, pp. 492–497, 1964.
- [33] K. Academy, "Neuron action potentials: The creation of a brain signal." <https://www.khanacademy.org/test-prep/mcat/organ-systems/neuron-membrane-potentials/a/neuron-action-potentials-the-creation-of-a-brain-signal>, June 2021.
- [34] A. L. Hodgkin and A. F. Huxley, "A quantitative description of membrane current and its application to conduction and excitation in nerve," *Physiology*, vol. 115, pp. 500–544, 1952.
- [35] E. Izhikevich, *Dynamical systems in neuroscience: the geometry of excitability and bursting*. MIT Press, 2010.
- [36] W. Gerstner, W. M. Kistler, R. Naudan, and L. Paninski, *Neuronal dynamics : from single neurons to networks and models of cognition*. Cambridge, 2014.
- [37] L. F. Abbott and C. van Vreeswijk, "Asynchronous states in a network of pulse-coupled oscillators," *Phys. Rev.*, vol. 48, pp. 1483–1490, 1993.
- [38] W. Gerstner and J. L. van Hemmen, "Associative memory in a network of 'spiking' neurons," *Phys. Rev.*, vol. 3, pp. 139–164, 1992.
- [39] B. W. Knight, "Dynamics of encoding in a population of neurons," *Phys. Rev.*, vol. 59, p. 734–766, 1972.
- [40] H. R. Wilson and J. D. Cowan, "Excitatory and inhibitory interactions in localized populations of model neurons," *Biophys.*, vol. 12, pp. 1–24, 1972.
- [41] X. Illa, B. Rebollo, G. Gabriel, M. V. Sánchez-Vives, and R. Villa *Progress in Biomedical Optics and Imaging - Proceedings of SPIE*, S. van den Driesche, Ed. (International Society for Optics and Photonics, 2015), vol. 9518, p. 951803.
- [42] M. D'Andola, J. F. Weinert, M. Mattia, and M. V. Sanchez-Vives, "Modulation of slow and fast oscillations by direct current stimulation in the cerebral cortex in vitro," *bioRxiv*, 2018.
- [43] D. A. El Boustani S, "A master equation formalism for macroscopic modeling of asynchronous irregular activity states.,," *Neural Comput.*, pp. 46–100, 2009.
- [44] A. Kuhn, A. Aertsen, and S. Rotter, "Neuronal integration of synaptic input in the fluctuation-driven regime," *Journal of Neuroscience*, vol. 24, no. 10, pp. 2345–2356, 2004.
- [45] C. A. Anastassiou, S. M. Montgomery, M. Barahona, G. Buzsáki, and C. Koch, "The effect of spatially inhomogeneous extracellular electric fields on neurons," *Journal of Neuroscience*, vol. 30, no. 5, pp. 1925–1936, 2010.
- [46] R. Reig, M. Mattia, A. Compte, C. Belmonte, and M. V. Sanchez-Vives, "Temperature modulation of slow and fast cortical rhythms," *J Neurophysiol*, vol. 103, pp. 1253–1261, Mar 2010.

A. Mean-field model (original) parameters

Symbol	Name	Value	Unit
Ω	Normalized spatial frequency of extracellular field	0.001	-
ϕ_s	Spatial phase of extracellular field	0	-
L	Normalized cable length	2	-
λ_{el}	Electrotonic constant	0.76	mm
E_0	Magnitude of electric field across layers	17	mV/m
σ_e	St. dev. of synaptic noise of E population	2000	Hz/ \sqrt{s}
σ_i	St. dev. of synaptic noise of I population	0	Hz/ \sqrt{s}
n_e	No of excitatory neurons	350	-
n_i	No of inhibitory neurons	87	-
τ_e	Time constant for excitatory population	10	ms
τ_i	Time constant for inhibitory population	5	ms
v_{ext}	Firing rate of external inputs	1000	Hz
δ_t	Integration time step	1	ms
g_L	Leak conductance	1/60	μs
B_e	Peak excitatory conductance	7.1	ns
B_i	Peak inhibitory conductance	3.7	ns
T_e	Time constant for excitatory population	0.2	ms
T_i	Time constant for inhibitory population	2	ms
E_I	Reversal potential of peak current	-70	mV
E_e	Reversal potential for excitatory currents	0	mV
E_i	Reversal potential for inhibitory currents	-75	mV
C	Membrane capacitance	250	pF
θ_e	Threshold for excitation	-50	mV
θ_i	Threshold for inhibition	-51	mV
τ_{adapt}	Adaptation time constant	800	ms
β_τ	Adaptation strength	0.05	$\mu V/Hz$
$\gamma_{epaptic}$	Ephaptic coupling	1/60	$\mu V/Hz$

Table 1: Estimated parameters in Rebollo *et al.* article [31]

B. Averaged recording results

		Up (s)	Down (s)	Frequency (Hz)
-3 V/m	0	0,182	6,617	0,302
	45	0,201	5,029	0,304
	90	0,234	3,165	0,436
0 V/m	0	0,220	3,465	0,467
	45	0,196	3,442	0,479
	90	0,255	3,429	0,412
3 V/m	0	0,160	1,986	0,837
	45	0,173	2,344	0,606
	90	0,185	3,573	0,432

Table 2: Averaged metrics extracted from the recorded data. Source: Sanchez-Vives laboratory

C. Parameter set results

Position	Tau (s)	Beta (uV/Hz)	Loss
1	1,4	0,3	0,327343189
2	1,5	0,3	0,352090823
3	0,7	0,35	0,430516756
4	1,6	0,15	0,485334111
5	0,7	0,15	0,48839233
6	0,9	0,15	0,507431338
7	1,3	0,3	0,53547121
8	1,6	0,3	0,584103321
9	0,8	0,15	0,607717564
10	1,2	0,15	0,612429463
11	1,1	0,15	0,61307582
12	1	0,15	0,713684814
13	1,5	0,15	0,766666797
14	1,4	0,15	0,773649561
15	1,3	0,15	0,967817282
16	1,2	0,3	1,160157629
17	0,7	0,25	1,613702789
18	0,8	0,25	1,741776049
19	1,1	0,3	1,867419147
20	0,8	0,35	1,869700542
21	1,2	0,25	2,698451421
22	0,9	0,35	2,705107004
23	1,1	0,25	2,706276199
24	1,6	0,25	2,79578041
25	1,5	0,25	2,815405034

Table 3: Sorted parameter set and loss obtained with the parameter search algorithm with weights: $\{w_{down}: 1, w_{up}: 1, w_{freq}: 0\}$.

D. Mean-field model implementation

```

1 import attr
2 import numpy as np
3
4 # SI base units
5 s = 1
6 kg = 1
7 m = 1
8 A = 1
9
10 # derived units
11 S = s**3*A**2/(kg*m**2)
12 V = kg*m**2*s**-3*A**-1
13 F = s**4 * A**2 * m**-2 * kg ** -1
14 Hz = 1/s
15
16 # with prefixes
17 nS = 1e-9 * S
18 uS = 1e-6 * S
19 mV = 1e-3 * V
20 uV = 1e-6 * V
21 pF = 1e-12 * F
22 ms = 1e-3 * s
23 nA = 1e-9 * A
24 pA = 1e-12 * A
25
26
27 def kuhn_transfer_function(threshold, tau_eff, mu_u, sigma_sq_u):
28     return 1. / (2 * tau_eff) * (special.erfc((threshold - mu_u) /
29                                         (np.sqrt(2) * np.sqrt(sigma_sq_u))))
30
31
32 def derivative_kuhn_transfer_function(threshold, tau_eff, mu_u, sigma_sq_u):
33     return 1. / (2 * tau_eff * (np.sqrt(2 * sigma_sq_u)) * (2 / np.sqrt(np.pi)) *
34                 np.exp(-(threshold - mu_u) ** 2 / (2 * sigma_sq_u)))
35
36
37 @attr.s
38 class EIMeanField:
39     E_e = attr.ib(0 * mV)
40     E_i = attr.ib(-75 * mV)
41     E_l = attr.ib(-70 * mV)
42     g_l = attr.ib(1./60 * uS)
43     C = attr.ib(250 * pF)
44     v_reset = attr.ib(-60 * mV)
45     threshold = attr.ib(-50 * mV)
46     threshold_inh = attr.ib(-53 * mV)
47     tau_ref = attr.ib(2 * ms)
48     T_e = attr.ib(0.2 * ms) # width of excitatory PSC (ms)
49     T_i = attr.ib(2 * ms) # width of inhibitory PSC (ms)
50     tau_e = attr.ib(1 * ms) # timescale of excitatory population (ms)
51     tau_i = attr.ib(0.5 * ms) # timescale of inhibitory population (ms)
52     B_e = attr.ib(7.1 * nS) # peak excitatory conductance (nS)
53     B_i = attr.ib(3.7 * nS) # peak inhibitory conductance (nS)
54
55     f_ext = attr.ib(5000 * Hz) # extracellular_firing_rate
56
57     n_e = attr.ib(350.) # number of excitatory neurons
58     n_i = attr.ib(350. / 4.) # number of inhibitory neurons
59
60     noise_std_e = attr.ib(2000 * Hz / np.sqrt(s))
61     noise_std_i = attr.ib(0 * Hz / np.sqrt(s))
62

```

```

63 tau_adapt = attr.ib(800 * ms) # adaptation time constant
64 beta_adapt = attr.ib(0.00005*mV / Hz) # strength of adaptation (per firing rate of E population)
65
66 def calc_membrane_stats(self, fr_e, fr_i):
67
68     mu_ge = fr_e * self.B_e * self.T_e * np.exp(1)
69     mu_gi = fr_i * self.B_i * self.T_i * np.exp(1)
70
71     gtot = self.g_l + mu_ge + mu_gi
72
73     mu_u = (self.E_l * self.g_l + self.E_e * mu_ge + self.E_i * mu_gi) / gtot
74
75     tau_eff = self.C / gtot
76
77     epsp_int = (self.E_e - mu_u) * self.B_e * self.T_e * np.exp(1) * tau_eff / self.C
78     ipsp_int = (self.E_i - mu_u) * (self.B_i * self.T_i * np.exp(1) * tau_eff / self.C)
79     epsp_sq = epsp_int ** 2 * (2 * tau_eff + self.T_e) / (4 * (tau_eff + self.T_e)**2)
80     ipsp_sq = ipsp_int ** 2 * (2 * tau_eff + self.T_i) / (4 * (tau_eff + self.T_i)**2)
81     sigma_sq_u = fr_e * epsp_sq + fr_i * ipsp_sq
82
83     return gtot, mu_u, tau_eff, sigma_sq_u
84
85
86 def calc_output_rate_inh_exc(self, fr_e, fr_i, delta_v_e=0, delta_v_i=0):
87     gtot_exc, mu_u_exc, tau_eff_exc, sigma_sq_u_exc = \
88         self.calc_membrane_stats(fr_e=fr_e, fr_i=fr_i)
89     gtot_inh, mu_u_inh, tau_eff_inh, sigma_sq_u_inh = \
90         self.calc_membrane_stats(fr_e=fr_e, fr_i=fr_i)
91
92     rexc = kuhn_transfer_function(self.threshold + delta_v_e,\n93                                 tau_eff_exc, mu_u_exc, sigma_sq_u_exc)
94     rinh = kuhn_transfer_function(self.threshold_inh + delta_v_i,\n95                                 tau_eff_inh, mu_u_inh, sigma_sq_u_inh)
96
97     return rexc * self.n_e, rinh * self.n_i
98
99 def ode_step(self, dt, rexc, rinh, theta_adapt, dv_e=0, dv_i=0):
100    fexc, finh = self.calc_output_rate_inh_exc(rexc + self.f_ext,\n101                                              rinh, theta_adapt + dv_e, dv_i)
102    theta_adapt = theta_adapt + (-theta_adapt +
103        self.beta_adapt * rexc) *\n104        dt / self.tau_adapt)
105    rinh = rinh + (-rinh + finh) * dt / self.tau_i
106    rexc = rexc + (-rexc + fexc) * dt / self.tau_e
107
108    return rexc, rinh, theta_adapt
109
110 def sde_step(self, dt, rexc, rinh, theta_adapt, dv_e=0, dv_i=0):
111    rexc, rinh, theta_adapt = self.ode_step(dt, rexc, rinh, theta_adapt, dv_e, dv_i)
112    rexc += np.random.randn() * self.noise_std_e * np.sqrt(dt)
113    rinh += np.random.randn() * self.noise_std_i * np.sqrt(dt)
114    rexc = np.maximum(rexc, 0)
115    rinh = np.maximum(rinh, 0)
116
117    return rexc, rinh, theta_adapt

```

Source Code 1: Core implementation of the model and the necessary functions to run the integration. To get access to execution examples of this code and ready to use notebooks see appendix F.

E. Signal processing methods

```

1  from collections import Counter
2  from numpy.fft import rfft
3  import math
4
5  # SIGNAL PROCESSING METHODS
6  # To compute the mua and moving variance
7
8  def decimate(signal, R=6):
9      # By default 6 factor downsample since 9900/6=1650 Hz is all the frequency resolution
10     # we need for the mua computation
11     pad_size = math.ceil(float(signal.size)/R)*R - signal.size
12     signal_padded = np.append(signal, np.zeros(pad_size)*np.NaN)
13     signal_padded.reshape(-1, R)
14
15     deci = signal_padded.reshape(-1, R).mean(axis=1)
16     return deci
17
18 def get_i_fft(yf, f):
19     return int(yf.size*f/(sampling_freq/2))
20
21 def compute_power(signal):
22     yf = np.abs(rfft(signal))
23     yf = yf
24     sq = yf*yf
25
26     i200, i1500 = get_i_fft(yf, 200), get_i_fft(yf, 1500)
27     sq_sum = np.sum(sq[i200:i1500])/(i1500-i200)
28     return sq_sum
29
30 def compute_mua(signal, sampling_freq, time_bin=20*ms):
31     mua = []
32     fft_period = time_bin*sampling_freq
33     i = 0
34     while True:
35         ix, iy = int(fft_period*i), int(fft_period*(i+1))
36         if ix<len(sub):
37             power = compute_power(sub[ix:iy])
38             mua.append(power)
39             i+=1
40         else:
41             return mua
42
43 def compute_moving_var(line, sampling_freq, window=100*ms):
44     ts = pd.Series(line, index=np.linspace(1,line.size,line.size))
45
46     samples = int(window*sampling_freq)
47     rolling_var = ts.rolling(window=samples).var().values
48     rolling_var = rolling_var[~np.isnan(rolling_var)] # This deletes first nan values
49
50     return rolling_var
51
52 # POST-PROCESSING METHODS
53 # To compute statistics for further study of the signals. Frequency computed as #peaks/time.
54 # The same methods are used to analyze the computer simulations of the model.
55
56 def count_peaks(signal, thr_val=3000, ones=250):
57     # 1.moving average
58     signal = signal
59     signal = np.convolve(signal, np.ones(ones))/ones
60     # 2.threshold the signal
61     thr = signal>thr_val
62     # 3.count ascending jumps

```

```

63     thr_array = thr.astype('int')
64     # 3.1 Computes the crossing 1: ascendent -1: descendent
65     difference = thr_array[1:]-thr_array[:-1]
66     # 3.2 Count the number of 1 (ascendent crossings)
67     peaks = Counter(difference)[1]
68     return thr_array, peaks
69
70 def periods(thr_array, time):
71     difference = thr_array[1:]-thr_array[:-1]
72     ups = np.where(difference==1)[0]
73     downs = np.where(difference== -1)[0]
74
75     sample = time/thr_array.size
76
77     # edge cases
78     # if one peak detected down time from down to end
79     # if no peaks detected up=0 down=time
80     up_periods = (downs-ups)*sample
81     down_periods = (ups[1:]-downs[:-1])*sample
82
83     if len(ups)==0:
84         up_periods = [0]
85         down_periods = [0]
86     elif len(ups)==1:
87         down_periods = [0]
88
89     return np.nanmean(up_periods), np.nanmean(down_periods)

```

Source Code 2: Implementation of various signal processing methods. The first block of functions are exclusively used with the experimental in vitro recordings. The second block are used for both the experimental and the computer simulated signals. To get access to execution examples of this code and ready to use notebooks see appendix F.

F. Open access Git repository

During the development of this thesis we spent some time learning about computational neuroscience models and scientific programming. And, while we found a big emphasis on the theoretical aspects of the publications, there were little to no publications that made some effort in order to improve the reproducibility of the publication. Thus making the learning part much more difficult, since there was no way to interact with the model and analyse the results. We want to give our little contribution to the field by giving open access to all the code used for the development of this thesis. In the following **link** (<https://github.com/jaumecolomhernandez/neuroscience-master-thesis>) there is an open access GitHub repository with code for the model implementation, the drivers for the data generation, the signal processing methods and all the plots in this document.